AD-A042 446 L N K CORP SILVER SPRING MD F/G 4/2
SEVERE STORM PATTERN RECOGNITION FROM METEOROLOGICAL SATELLITE --ETC(U)
JUN 77 L N KANAL, J A PARIKH DAAG29-76-D-0100
UNCLASSIFIED ECOM-77-3 NL

1 OF 2
AD
A042446

Code 23

13 B.S.

RESEARCH AND DEVELOPMENT TECHNICAL REPORT
ECOM-77-3

SEVERE STORM PATTERN RECOGNITION FROM METEOROLOGICAL SATELLITE DATA
A Report on Current Status and Prospects

By

Laveen N. Kanal
Jo Ann Parikh
L.N.K. Corporation
302 Notley Court
Silver Spring, MD 20904

Contract Monitor: Bruce Miers

Atmospheric Sciences Laboratory
US Army Electronics Command
White Sands Missile Range, New Mexico 88002

June 1977

Approved for public release; distribution unlimited.

ECOM
UNITED STATES ARMY ELECTRONICS COMMAND - FORT MONMOUTH, NEW JERSEY 07703

NOTICES

Disclaimers

The findings in this report are not to be construed as an official Department of the Army position, unless so designated by other authorized documents.

The citation of trade names and names of manufacturers in this report is not to be construed as official Government indorsement or approval of commercial products or services referenced herein.

Disposition

Destroy this report when it is no longer needed. Do not return it to the originator.

SECURITY CLASSIFICATION OF THIS PAGE *(When Data Entered)*

REPORT DOCUMENTATION PAGE

READ INSTRUCTIONS BEFORE COMPLETING FORM

1. REPORT NUMBER: ECOM-77-3	2. GOVT ACCESSION NO.
3. RECIPIENT'S CATALOG NUMBER	
4. TITLE *(and Subtitle)*: SEVERE STORM PATTERN RECOGNITION FROM METEOROLOGICAL SATELLITE DATA, A Report on Current Status and Prospects.	5. TYPE OF REPORT & PERIOD COVERED: Final Report.
	6. PERFORMING ORG. REPORT NUMBER
7. AUTHOR(s): Laveen N. Kanal, Jo Ann Parikh	8. CONTRACT OR GRANT NUMBER(s): DAAG29-76-D-0100
9. PERFORMING ORGANIZATION NAME AND ADDRESS: L. N. K. Corporation, 302 Notley Court, Silver Spring, MD 20904	10. PROGRAM ELEMENT, PROJECT, TASK AREA & WORK UNIT NUMBERS: DA Task 1T162111AH71
11. CONTROLLING OFFICE NAME AND ADDRESS: US Army Electronics Command, Fort Monmouth, NJ 07703	12. REPORT DATE: June 1977
	13. NUMBER OF PAGES: 115
14. MONITORING AGENCY NAME & ADDRESS *(if different from Controlling Office)*: Atmospheric Sciences Laboratory, US Army Electronics Command, White Sands Missile Range, NM 88002	15. SECURITY CLASS. *(of this report)*: UNCLASSIFIED
	15a. DECLASSIFICATION/DOWNGRADING SCHEDULE

16. DISTRIBUTION STATEMENT *(of this Report)*

Approved for public release; distribution unlimited.

17. DISTRIBUTION STATEMENT *(of the abstract entered in Block 20, if different from Report)*

18. SUPPLEMENTARY NOTES

19. KEY WORDS *(Continue on reverse side if necessary and identify by block number)*

Pattern recognition
Severe storms
Cloud classification
Cloud geometry
Cross-correlation methods

20. ABSTRACT *(Continue on reverse side if necessary and identify by block number)*

This report presents the results of a preliminary study on severe storm feature recognition from visible and infrared meteorological satellite data. Pattern recognition models are reviewed and satellite-derived features for various categories of severe weather are enumerated and described. The detection and tracking of severe storm features are discussed in terms of cloud classification and segmentation, cloud geometry, and cloud tracking. The current status and potential feasibility of pattern recognition techniques for severe storm feature identification are assessed.

DD FORM 1 JAN 73 1473 EDITION OF 1 NOV 65 IS OBSOLETE

SECURITY CLASSIFICATION OF THIS PAGE *(When Data Entered)*

391 718

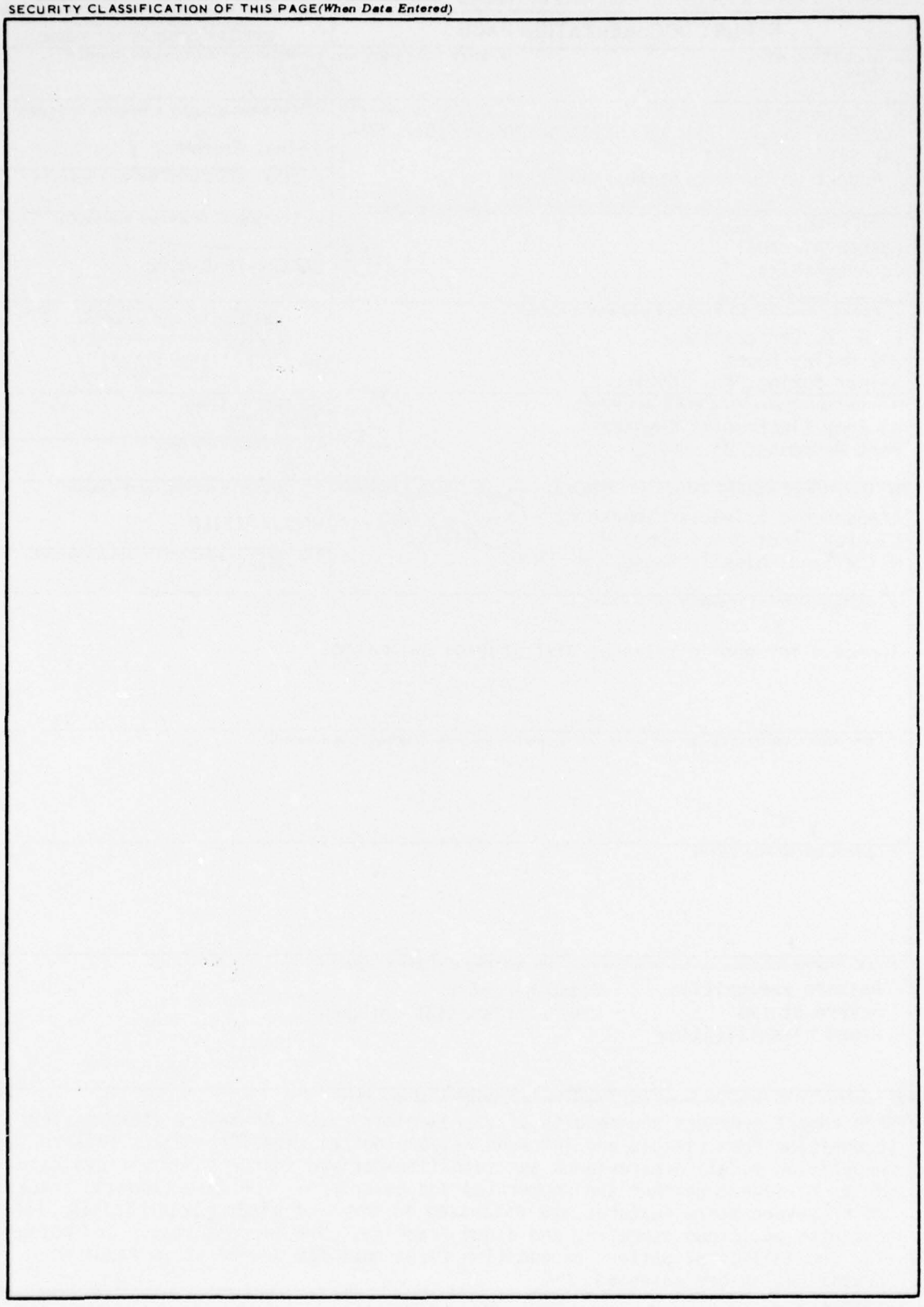

Preface

This work was performed under Contract DAAG29-76-D-0100, D.O. No. 0103 for scientific services, by Laveen N. Kanal and Jo Ann Parikh. Bruce Miers, DRSEL-BL-MS, Atmospheric Sciences Laboratory, U.S. Army Electronics Command, White Sands Missile Range, N.M., served as the cognizant technical monitor.

The authors are grateful to Robert F. Adler, NASA Goddard, and James F.W. Purdom and Roderick A. Scofield, National Environmental Satellite Service, NOAA, for extensive discussions which proved most helpful in the initial stages of this study. The authors are also grateful to Ralph K. Andersen, and James J. Gurka, NESS, Jerome P. Charba, National Weather Service, NOAA, D. K. Lilly, National Center for Atmospheric Research, Colorado, Robert G. Miller, and Rance Skidmore, Air Weather Service, Scott AFB, Richard G. Savage, AF Global Weather Central OFFUT AFB, Nebraska, and William E. Shenk, NASA Goddard for assistance in providing references, and responding most kindly to telephone calls and/or written questionnaires.

TABLE OF CONTENTS

APPLICATION OF PATTERN RECOGNITION TECHNIQUES TO DETECTION OF SEVERE STORM FEATURES FROM METEOROLOGICAL SATELLITE DATA

0. Introduction

The availability of high-resolution satellite imagery from SMS/GOES offers a unique opportunity to monitor severe weather phenomena on the mesoscale. The objectives of this report are to summarize features of various categories of severe storms and examine the applicability of pattern recognition techniques to the identification and prediction of severe storms from visible and infrared satellite imagery.

Pattern recognition models for severe weather phenomena differ from classical, statistical pattern recognition models in terms of feature values, stages of decision logic, branching logic, and feedback capability. Feature values are often discrete (representing the presence or absence of one or more events associated with severe weather) rather than continuous. The decision logic proceeds through various stages, often backing up or modifying previous decisions, until a final classification (such as number of inches of rainfall or cyclone intensity) is made.

The degree of automation which can be introduced into these pattern recognition systems can vary from total automation to a completely manual approach. The cost of development and/or application of automatic pattern techniques must be considered on an individual basis for each type of feature to be extracted. In general, those features which must be obtained by automatically tracking a sequence of cloud objects are more expensive than those which can be obtained from a single image.

This investigation began with a literature survey, a questionnaire, on-site visits to NASA and NESS and interviews with meteorologists expert in various aspects of severe storm identification and prediction. Section 1 reviews

the pattern recognition models relevant to severe storm identification and prediction. Section 2 summarizes for various categories of severe weather those features which characterize each category. The digitized data necessary to extract each feature is considered.

For a completely automatic system for severe weather pattern recognition models, algorithms for (1) cloud classification, (2) cloud segmentation, (3) cloud geometry, and (4) cloud tracking need to be developed. A review of algorithms in these four different areas and suggestions for future algorithmic development are presented in Section 3.

The concluding section outlines our recommendations on the feasibility and priority of development of some pattern recognition techniques for identification of severe weather features.

1. Pattern Recognition Models

One can consider a number of different paradigms for pattern recognition. A description of the major models serving to direct research on machine patterns appears in Kanal [1974]. The two main approaches are termed (a) the Feature Extraction-Classification model, and (b) the linguistic or syntactic model.

Feature Extraction Classification Model

In the feature extraction classification model, recognition is achieved by making measurements on the patterns to be recognized, and then deriving features from these measurements. These features form the input to a classification procedure that gives a class, group or category assignment for each pattern. The available information from the pattern environment is thereby reduced, in stages, ultimately to a small number of categories.

A commonly used version of the feature-extraction classification model is one in which the features are treated as components of a vector $X = (x_1, x_2, \ldots, x_n)$. Each pattern is considered to be a point in the resulting n-dimensional feature space. Classification is then treated as a problem of dividing this n-dimensional space into exclusive regions R_j, $j = 1,2\ldots k$, such that when a feature vector falls into R_j, the pattern is assigned to class j. This division might be effected on the basis of statistical or non-statistical considerations. Note that any type of feature may be used in this model.

In the simplest case where there is no variability within pattern classes, classification reduces to template matching in which an observed pattern is matched against a prototype (template). When the variability is limited, it may be possible to extend this idea to the feature space and classify patterns

according to their distance from the nearest prototype. In most problems one needs to employ more sophisticated methods of multivariate statistical classification for defining the regions R_j.

The Linguistic-Syntactic Model

The commonly used version of the feature-extraction classification model has been criticized for focusing primarily on statistical relationships among the features while ignoring other "structural" properties that seem to characterize patterns. Also the classification into a region R_j of n-dimensional space leads only to a class designation of a pattern rather than a description which provides some insight concerning the class, or which allows one to generate patterns belonging to a class.

Various approaches are being taken to overcome the above perceived failings of the feature-extraction classification model. In the linguistic model for pattern description, patterns are viewed as sentences in a language defined by a formal grammar. A "primitive extractor" transforms the input data into a string of symbols or some general relational structure. The primitive extractor may itself be a feature extractor classifier. Then a structural pattern analyzer uses a formal grammar to parse the string and thus constructs a description of the pattern.

The stress on the distinction between the feature-extraction classification model and the linguistic-syntactic model misses the obvious points that, even in the syntactic model, the primitives are features that have to be extracted from measurements, and that associating a pattern with a generative model is essentially equivalent to classifying the pattern into categories represented by the generative models. Clearly, the generative models need not be restricted to formal grammars. One could include such familiar models

as a differential equation model, a functional equation model, or a stochastic model such as a finite state Markov chain model.

Structural Pattern Recognition

When a formal model is not explicitly present, the terms "ad-hoc" or "heuristic" are used. The phrase "structural pattern recognition" refers to all pattern recognition approaches based on defining primitives and identifying allowable structures in terms of relationships among primitives, and substructures that combine primitives. The relations might be boolean expressions or might be specifiable by some statistical relationships or by a generative grammar model. The term structural pattern recognition represents less a specific set of procedures than an attitude, i.e., that pattern recognition algorithms should be based on the mechanisms that generate and deform patterns.

Hierarchical Classifiers

Hierarchical classifiers or decision trees have been used extensively in many application areas of multiclass pattern recognition. A hierarchy of classifiers provides a flexible way to incorporate different feature subsets, statistical, linguistic, or ad-hoc relationships, and decision policies at the various nodes of the tree.

All the problems of feature selection and classifier design are accentuated in the multiclass multimodal case, and the usual single stage multivariate linear or nonlinear discriminant function approach often fares more poorly than anticipated.

The apparent theoretical increase in discriminating ability of single stage nonlinear discriminant functions is usually not realizable in practice because of problems involved in estimating the fine structure, represented

by the higher-order relationships among the features, due to dimensionality and sample size considerations [See Kanal 1974].

In an M class problem, for a given sample size per class, dimensionality-sample size considerations may dictate that no more than n features be used. It is likely that the best set of n features to discriminante between one group of classes is quite different from the best n features for another set of classes. Limiting consideration to some n features to be used in a single step to make an M-way decision may lead to a forced compromise in the choice of the feature set. Splitting the decision into several stages might be better. Then at each stage of the decision process, the n features best suited for that classification task could be used. This permits the multi-class classification problem to be decomposed into a series of less complex decision problems. The optimal and heuristic design of decision trees which use both physical model-based features and data derived features is the subject of current research by Dr. Laveen Kanal and his students at the Laboratory for Pattern Analysis of the University of Maryland [e.g. Kulkarni 1976, Kulkarni and Kanal 1976].

In practice, the optimal techniques for designing decision trees are not feasible, and the various suboptimal techniques for tree design are best viewed as subroutines to be utilized in a recursive, interactive approach to the design of hierarchical classifiers. Reasons for taking an automated, interactive, graphics-oriented approach to pattern analysis and the design of classification systems were summarized in Kanal [1972], which also described a number of representative interactive pattern analysis and classification systems (IPACS) then implemented or under development.

MIPACS, the Maryland Interactive Pattern Analysis and Classification System which is partially implemented, was designed to facilitate the inter-

active design of single stage and hierarchical classifiers [Stockman and Kulkarni (1976), Kanal (1977)]. MIPACS has been found very useful by Ms. Jo Ann Parikh in interactively designing and testing decision trees for her dissertation on cloud classification and segmentation [Parikh (1977a, 1977b)].

We note here that (in unpublished work) Scofield has developed a decision tree for thunderstorms to aid human decision making (See Fig. 1), and D. Tarpley of NESS has developed a decision tree for recognition of low clouds.

For severe storm identification and recognition, it is clear that the classification model which will have to be relied upon is the hierarchical classifier or decision tree with statistical and other structural features and relationships being used at the various nodes. The design and testing of the classifiers for some of the severe storm features will have to be experimented within an interactive manner, before defining an operational procedure to be recommended for use in any automatic or semi-automatic system.

Some of the general problems of pattern recognition, which affect the development of pattern recognition schemes for a variety of application areas, were listed in Kanal [1975]. Some of those problems impinge upon the development of automatic and semi-automatic systems for severe storm feature extraction and classification. Additional problems arise in the severe storm area from the fact that some of the important features which are used or may be potentially used to identify severe storm activity are not defined in a static manner. Rather many features are defined by the nature of their evolution in time, with the time involved ranging from a fraction of an hour to days. Procedures for the automatic extraction of such time dependent

features, many of which are described in subsequent sections, are essentially lacking in the published literature on digital picture processing [Rosenfeld and Kak (1976)]. It does seem feasible to develop automatic procedures for some of the more important time dependent features, and these are taken up in Section 3.4 and in the recommendations. Many of the available procedures for curve detection, line detection, description of pattern geometry, and pattern segmentation, some of which are discussed in Section 3, need to be examined in a comparative study for their relevance to severe storm feature detection. The state of the art of image pattern recognition is unfortunately not so advanced that one can decide without experimentation on real data which procedure is best for a given application.

2. Description of Severe Weather Features.

A compilation of severe weather features by severe storm category was prepared from information obtained from a review of the literature, consultations with satellite meteorologists, and responses from a questionnaire. The format of the questionnaire is presented in the appendix. The responses received are reflected in the text of this report.

Four categories of severe storms were of major interest to the satellite meteorologists:

1) Severe windstorm
2) Heavy rainstorm
3) Hailstorm
4) Tornado

Two other categories of severe storms--blizzards and electrical storms (lightning)--will not be considered in this study. Blizzards tend to be characterized by larger scale features than the mesoscale features which have been used to identify and/or predict severe windstorms, etc. Further research is needed before definitive correlations between specific satellite features and the occurence of severe electrical storms can be made. Many of the features which are relevant to the severe storm categories above will probably prove to be of importance in the case of electrical storms.

A list of severe weather features resulting from merging the responses to the questionnaire on this topic is given in Table 1. An attempt was made to place the most important features for each storm category near the top of the list.

Most of the features can be detected from observations of a sequence of infrared or enhanced infrared images. Included among these features are

splitting cells, merging cells, speed-of-cell movement, vertical growth rate of cells, change in top heights and life cycles of overshooting tops. Wind fields which can be automatically extracted from visible or infrared sequences by cloud tracking algorithms can be used to determine low-level vorticity, patterns of upper-level divergence combined with low-level convergence, whether a storm is deviating to the right or left of the mean wind, and upper-level jets in the vicinity of storms. Specific cloud types or configurations associated with these features also can be used to identify their presence in a single image. Mesohigh boundary interactions, pendant-shaped cells, low-level cumulus cloud line feeder bands, the texture of a cell, and the location of the steepest temperature gradient are severe weather features which can be observed in a single image. Overshooting tops are, in general, too small to be observed in the infrared images where the resolution is 4 nautical miles (n.m.) but can be detected in the visible images where the resolution is 1/2 n.m. or 1 n.m.

A brief description of each of the features in Table 1 is included in this section. Algorithms to extract each feature are considered in Section 3. Section 3 provides insight into the nature of the problems which must be solved if a completely automatic system is to be developed.

2.1. Mesohigh Boundary Interaction

The intersection or merger of the outer boundary of a mesoscale high pressure system with another convective boundary (such as a front, squall line, or another mesohigh) was shown by Purdom [74,76a] to almost always result in an increase in convective activity. Rain, a decrease in temperature, a pressure surge, gust fronts, and tornado activity may occur at

Table 1. Meteorological Satellite Features for Characterization of Severe Storms

SEVERE STORM FEATURES	Severe Storm Category			
	Severe Windstorm	Heavy Rainstorm	Hailstorm	Tornado
	1. Speed-of-cell movement	1. Steepest temperature gradient	1. Overshooting tops	1. Mesohigh boundary interactions
	2. Steepest temperature gradient	2. Vertical growth rate of cell	2. Top heights	2. Right deviating storms
	3. Mesohigh Boundary interactions	3. Merging cells	3. Vertical growth rate of cell	3. Overshooting tops
	4. Right deviating storms	4. Slow moving storms or big storms moving over same place	4. Splitting cells	4. Positive low-level vorticity
	5. Overshooting tops	5. Bright textured	5. Right or left deviating storms	5. Vertical growth rate of cell
	6. Vertical growth rate of cell	6. Overshooting tops		6. Upper-level divergence and low-level convergence
	7. Upper-level jet in vicinity of storm	7. Low-level cumulus cloud-line feeder bands		7. Splitting cells
				8. Pendant-shaped cells

these points of convective intersection. There are two basic cloud patterns described by Gurka [76] which are associated with mesohighs. In the first case, the outer boundary of the mesohigh appears "as an oval shaped leading edge to the thunderstorm with the anvil cirrus curving anticyclonically out of the rear of the (thunderstorm) cluster". In the second case, the outer boundary appears as "an arc shaped line of convective clouds advancing outward from a dissipating thunderstorm area". The parent cumulonimbus cell may exhibit a "comma" tail.

The comma-shaped cloud pattern, which is associated with areas of upper tropospheric vorticity, is often indicative of severe weather. Mathews and Johnston [76] reported the occurrence of tornado activity, gust storms in excess of 50 knots, and hail in the area of a compact, well-organized comma cloud system. They attributed the severity of the thunderstorm outbreak to the relationship between well-defined comma cloud systems and concentrations of positive vorticity advection (strong upward vertical motion). Parmenter [76] described a rain/snow producing sub-synoptic system in which the cloudiness associated with a surface wave had a distinct comma shape with colder tops along the northern side.

In order to determine or differentiate areas of severe weather along the mesohigh boundary, Gurka [76] recommended in the case of gust fronts use of enhanced infrared and visible imagery to locate features such as temperature of the coldest tops in the thunderstorm cluster behind the mesohigh boundary, the presence of overshooting tops, cloud edge gradients, and speed of motion of the arc bounding the mesohigh. The role of intersecting arc lines (mesohigh boundary interactions) was also emphasized.

2.2. Low-Level Cumulus Cloud Line Feeder Bands

Low-level cumulus cloud line feeder bands refer to the mesoscale lines of small cumulus clouds which move or feed into a thunderstorm system, maintaining and replenishing the moisture of the thunderstorm system. These cloud lines represent areas of low-level moisture convergence. When these convective lines intersect or merge into another convective boundary or line, enhanced thunderstorm activity almost always results. An example of this type of merger appeared in Purdom [74]. The location of new thunderstorms along the cloud line of an old mesohigh boundary was shown to coincide with the point where low-level cumulus lines merged into it from the south.

The recognition of convective lines in satellite imagery plays a major role in the prediction of thunderstorm activity. Oliver and Purdom [74] stated that "almost all new large convective activity in the tropics forms on a pre-existing line". They differentiated various types of line patterns in satellite imagery including synoptic frontal bands, squall lines, rope-like clouds, and mesoscale lines of small cumulus clouds. Convective lines representing areas of low-level moisture convergence may be terrain related. However, Purdom [74] noted: "Regardless of the generation mechanism for a convective boundary or line, when it merges with and intersects another convective boundary or line, more intense convective activity almost always results."

2.3. Steepest Temperature Gradient

The location of a gust front along the leading edge of a cumulonimbus system and the area of most significant precipitation in a convective system can be determined by analysis of the temperature gradients within the thunderstorm systems. Gurka [76] noted that "the gust front is usually located

very close to the strongest temperature gradient in the infrared pictures, near the leading edge of the cumulonimbus". Oliver and Scofield [76] observed that the area of most significant precipitation (which may consist of only one-tenth or less of the entire anvil area) in a convective system occurred in the upwind portion of the system. The upwind portion of the convective system can be determined in a single enhanced infrared image from the shape of the individual anvils and the location of the steepest temperature gradient. Anvil cirrus has a distinct sharp edge on the upwind side and a fuzzy edge downwind. The plumes often extend downwind several degrees. The location of the largest temperature gradients in images formed by summing digital values for enhanced infrared images over a 6-hour period can also be used to determine the upwind portion of the convective system. A high degree of correlation (correlation factor of 0.88) was obtained by Oliver and Scofield [76] between observed 6-hour precipitation and cumulative digital infrared values in the upwind portion of the convective system.

Enhanced infrared imagery is used to "better display low clouds, to better identify the structure of convective storms and to locate sea-surface temperature gradients" (Anderson[74]). Enhanced infrared images are obtained by transforming the gray-scale of infrared images by application of specific enhancement curves. Display devices for infrared imagery are, in general, limited from 16 gray shades (or less for facsimile recorders) to 64 gray shades. If infrared imagery is not enhanced, temperature increments are equal for each shade of gray in the display. In order to enhance the data, the range of possible temperature values is partitioned into temperature intervals or segments and for each segment a linear mapping from the temperature values within the segment to a specific gray scale range is specified.

If no enhancement is desired for the segment, the linear function consists of a straight line with slope factor 1. The enhancement curve may assign gray shades out of sequence instead of varying gray shades from black to white as the temperature decreases. This type of enhancement (alternating light and dark shades) is particularly effective for identifying the structure of convective storms. The enhanced infrared pictures used by Gurka [74] were produced by assigning gray shade values to temperature intervals as specified below:

+30°C to -44°C	-- linear assignment from black to near white
-45°C to -57°C	-- dark gray
-58°C to -63°C	-- light gray
colder than -63°C	-- black

The following enhancement procedure was used by Oliver and Scofield [76] for summer convection in the middle latitudes:

+17° to -2°C	-- dark gray
-3° to -23°C	-- light gray
-24°C to -43°C	-- white
-44°C to -58°C	-- dark gray
-59°C to -63°C	-- light gray
-64°C to -68°C	-- blackest
below -68°C	-- whitest

A comparison of three enhancement curves for GOES-1 infrared imagery available in the Washington Satellite Field Services Station on February 1976 can be found in Clark [76].

The location of the steepest temperature gradient in enhanced infrared imagery is determined by observing a narrowing of the width or distance between gray shade contours. According to Scofield [76], "There are situations when the upwind portion (area of tight IR temperature gradient) and active thunderstorm clusters are difficult to find because: (1) the tight IR temperature gradients cannot be discerned, or (2) the colder enhanced IR contours overspread a large area." There is clearly a need to incorporate pattern re-

cognition techniques for analysis of infrared gradients into a system for producing enhanced infrared imagery. The need to develop pattern recognition techniques that enhance and identify the surface thermal gradients was discussed by Miller et al. [75] under the heading of "Severe Storm Potential Analysis". They recommended use of thermal gradient maps to quantify phenomena such as the motion of arc clouds and to delineate "the relative hot and cold 'tongues' that seem to be necessary conditions for certain kinds of severe weather generation".

2.4. Top Heights

"The highest and coldest clouds form where the thunderstorms are most vigorous" (Oliver & Scofield [76]). Near the convective cells with the coldest tops the strongest winds, the heaviest rain, and the most severe thunderstorm activity occur. An outbreak of severe weather in the Midwest which produced 4 tornadoes, 14 occurrences of gusts in excess of 50 knots, wind damage, and hail up to golf ball size was found by Mathews and Johnston [76] to be associated with a comma cloud pattern in which cloud tops up to 46,000 ft. were indicated by radar.

The height of cloud tops can be obtained from the cloud-top temperatures and a vertical temperature profile of the area of interest. Procedures to determine cloud-top temperatures from satellite radiance measurements generally make two basic assumptions: (1) clouds are opaque and hence their emissivities are equal to unity, and (2) a constant correction factor may be applied for water vapor contributions above the cloud. Liou [75] noted that both assumptions seem justified for cumulonimbus clouds which are fairly high in the atmosphere but added that "it seems unlikely that a cloud whose emissivity equals unity may be isolated from satellite observations", and

that "unless a reliable radiative transfer calculation can be carried out, the uncertainties of the emissivity of thick clouds or multilayered clouds may lead to serious errors in the evaluation of cloud-top temperatures." If the field of view of the satellite sensor is not completely filled by clouds which are sufficiently dense to shield the satellite sensor from radiation below the cloud, the radiance at the satellite will represent the sum of radiance from the cloud and radiance from surfaces beneath the cloud. If other types of clouds are also in the field of view, for example, layer-type clouds such as cirrostratus and altostratus, the assumption of an emissivity of 1.0 may not be valid. Discussions of relationships between cloud-top temperatures, brightness, and heights can be found in Mosher [76], Shenk and Curran [73], Park et al. [74], Gruber [75], Liou [75], and Young [75]. The cloud height program of Mosher [76] determines the height of wind tracer clouds by using visible brightness, solar zenith angle, satellite zenith angle, relative azimuth angle, cloud type (ice or water clouds), etc., to calculate cloud emissivity as a function of the optical thickness of a cloud. Further investigation is needed to determine whether or not within a thunderstorm system areas of coldest satellite radiance measurements can be equated with areas of coldest cloud tops (i.e., if the assumption of cloud emissivity equal to unity suffices) or if more complicated algorithms, such as the cloud height algorithm of Mosher [76], need to be implemented.

2.5. Vertical Growth Rate of Cell

The vertical growth rate of a cell is determined from enhanced infrared imagery by observing the change of satellite radiance measurement with time. Assuming that the changes in radiance measurements parallel changes in temperature and that temperature decreases with height, then the expansion of a

gray shade contour representing the coldest radiance measurements denotes a vertical growth of the cell. The rate of growth is represented by the change in area of this contour over the time period of interest. This change will be a function of the particular enhancement curve used to produce the enhanced imagery.

The amount of expansion (measured in terms of degrees of latitude) of cloud tops in the upwind portion of a convective system was one of the factors in Scofield's decision tree procedure (Fig. 1) which contributed toward an increase in the amount of convective rainfall. Larger amounts of precipitation were associated with colder tops and with rapidly expanding tops. Winds of 50 knots were reported in the area of a cloud pattern typical of air mass thunderstorms when the parent cumulonimbus cell was rapidly growing and producing heavy rainfall (Gurka [74]).

2.6. Overshooting Tops

Overshooting tops refer to thunderstorm tops which "shoot over" or above the anvil portion of the thunderstorm. The upper limit of thunderstorm growth is determined by the height of the stratosphere. The tropopause, the base of the stratosphere, is defined as "the level at which temperature begins to increase with height or at least decreases at a rate below 1.1°F. per 1000 ft. (Battan [61]). When the cloud air moves into the stratosphere, it will be subjected to a downward force since the ascending air is colder and hence more dense than the surrounding air. The updraft speeds in the thunderstorm, however, may be so high that the upward momentum will propel the cloud air several thousand feet above the tropopause until the downward force brings it to a halt.

Overshooting tops can be recognized from both visible and infrared imagery. The presence of overshooting tops in infrared imagery can be ascertained by determining if the cloud-top temperature is higher than the temperature of the tropospause at the given location. Miller et al [75] suggested that overshooting tops may be "delineated by simple gradient or curvature enhancement techniques". A second indication of overshooting tops is the appearance of an uneven or lumpy texture within the thunderstorm system. Individual overshooting tops are usually too small to be seen in infrared imagery (4-mile resolution). If visible imagery (1/2- or 1-mile resolution) is available, overshooting tops can be detected by the shadow they cast upon the anvil.

Overshooting tops are associated with the most hazardous parts of thunderstorms. If a cloud is capable of producing large hailstones, it must have very strong updrafts. These updrafts would furnish the upward momentum to produce overshooting tops. According to Battan [61], if a hailstone is to reach a diameter of 3 inches, it must take several trips to the top of a tall thunderstorm and down again. Since a 3-inch hailstone has a fall speed of about 6000 feet per minute, vertical motions of this magnitude must exist within the cloud. When analyzing cloud patterns associated with strong wind zones, Gurka [74] stated that "on visible imagery, the strongest cells can sometimes be located by overshooting tops above the anvil." Scofield's decision tree procedure (Fig.1) for half hourly estimation of convective rainfall increases the half hourly estimated amount of precipitation by 0.50 inch if overshooting tops (located on visible imagery) occurred in the upwind portion of a thunderstorm system. For an example of visible imagery showing a line of overshooting tops in a thunderstorm cluster, see Scofield

2.7. Bright Textured

Thunderstorm clouds which produce the heaviest precipitation appear bright and textured in the visible imagery. Bright, smooth clouds are often representative of middle and high cloud debris without precipitation (Scofield [76]). Darker clouds and translucent clouds also are not generally indicative of heavy amounts of falling precipitation. In addition to a bright-textured appearance, features which can be extracted from visible imagery for characterization of heavy rainstorms include overshooting tops, merging thunderstorms (also can be observed in enhanced infrared), and low-level cumulus cloud-line feeder bands.

2.8. Upper-Level Jet in Vicinity of Storm

A jet stream is defined by the World Meteorological Organization (WMO) as "a strong narrow current, concentrated along a quasi-horizontal axis in the upper troposphere or in the stratosphere, characterized by strong vertical and lateral wind shears and featuring one or more velocity maxima". There are two main westerly jet streams at upper troposphere level: (1) the subtropical jet stream which is found between 30,000 and 40,000 feet above sea level between 30° and 35° latitude and (2) the circumpolar or polar jet stream located somewhat lower in the atmosphere and further away from the equator than the subtropical jet stream. According to the definition adopted by the World Meteorological Organization: "Normally a jet stream is thousands of kilometers in length, hundreds of kilometers in width and some kilometers in depth. The vertical shear of wind is of the order of 5 to 10 mps (1 meter per second = 2 knots) per kilometer, and the lateral shear is of the order of 5 mps per 100 km. An arbitrary lower limit of 30 mps is assigned to the speed of the wind along the axis of a jet stream". A jet

axis is the axis of strongest winds within a jet stream. Jet maxima (velocity maxima) are centers of high wind speed along the jet streams. Winds may reach more than 250 knots along a jet stream axis.

Location of a jet axis can be determined from satellite derived upper-level wind data or from examination of cloud patterns in the vicinity of the jet stream. Auvine and Sikdar [73] observed that "the jet axis closely follows the zero vorticity line with anticyclonic vorticity to the southeast and cyclonic to the northwest", which "was in accord with the theoretical expectation for a westerly jet stream". They used Mancuso and Endlich's [73] Wind Editing and Analysis Program to obtain a computer analysis of the divergence and relative vorticity fields. "The main jet-stream cloud features are long shadow lines, large cirrus shields with sharp boundaries, long cirrus bands, cirrus streaks, and transverse bands within cirrus cloud formations" (Anderson [74]). In order to locate on visible imagery the polar jet (which breeds blizzards and stormy weather over the United States), one should look for the sharp poleward edge of a large, slightly anticyclonically-curved cirrus shield. The shadow cast by the high jet-stream cirrus clouds on lower clouds or surface features usually extends far from the edge of the cloud. "Poleward from the jet streams the clouds present a 'lumpy' appearance, while on the equatorward side the clouds look much more even" (Anderson [74]). Relationships between synoptic features (such as jet streams) and representative cloud patterns, although generally valid, do not always apply in each specific instance. For example, Doswell and Schaeffer [76] reported a finding on May 4, 1975, in which the position of cirriform bands and streaks was well south of the jet core which was "at variance with the literature on satellite interpretation."

Middle and upper-level jets are often associated with outbreaks of severe weather. Anderson [74] pointed out that "an important factor in forecasting severe weather is the presence of a mechanism that produces upper-level divergence," and "in most cases this is a jet stream." Tornado outbreaks have occurred near the intersection of a low-level and upper-level jet (Miller [71]) and near the intersection of a dry line and a jet stream (Miller [76]). According to Anderson [74], "tornadoes occurring in the presence of the subtropical jet stream are normally beneath its intersection with the squall line and to the north of the jet axis." Scofield [75] traced a heavy snowstorm to an upper air disturbance in the vicinity of a 300-mb jet axis. Auvine and Sikdar [73] located the jet core to the west of storm regions which produced severe weather including tornadoes and located the jet axis to the northwest of the precipitation area. In the cases they studied, they found similar fluctuations between cirrus tracer motions near the jet stream and nearby severe storm intensity which suggested "some sort of direct interactions of the severe storm evolutions with the jet-stream flow field."

2.9. Pendant-Shaped Cells

Pendant-shaped cells or "carrot" cells refer to thunderstorm cells which develop in a strong, vertical shear environment. These thunderstorm cells, which are shaped by the veer of wind with height, are stretched out horizontally so that the elongated axis of the anvil is parallel to the vertical wind shear between the lower and upper troposphere. The vertical wind shear vector is parallel to the mid-tropospheric isotherms. Pendant-shaped cells often occur in close proximity to jet streams; typically, in the vicinity of a low-level southerly jet and a high-level westerly jet. The wind shift from southeast to south to southwest with height produces the characteristic

pendant shape of the cells.

Anderson [74] pointed out that "veering of winds with height is an important parameter in forecasting severe weather." NOAA-1 infrared imagery, depicting pendant-shaped cells in an area in which tornadoes occurred beneath the intersection of low- and mid-level jets, can be found in Figure 5-E-3 of Anderson [74]. Although pendant-shaped cells are generally associated with thunderstorms, their significance in determining the severity of a thunderstorm is questionable. Further statistical analysis is needed to evaluate the importance of including pendant-shaped cells as a feature in severe storm pattern recognition models.

2.10. Right (or Left) Deviating Storms

Right (or left) deviating storms are thunderstorm cells which move to the right (or left) of the mean tropospheric wind. Right moving (right deviating) storms often occur after a thunderstorm cell splits into two separate sections, with one section (left deviating) moving to the left of the mean wind and one section (right deviating) to the right. The right deviating, cyclonically rotating cell is associated with severe thunderstorms. "One of the characteristics of a convective system is for thunderstorm generation to take place on the upwind side and to propagate to the right of the mean tropospheric wind" (Scofield [76]).

The movement or deviation of a storm from the mean wind can be observed from sequences of enhanced infrared imagery. The coldest temperatures of the right deviating thunderstorm move to the right of the mean motion. The mean wind or wind direction can be determined by tracking appropriate cloud targets for wind velocity estimation. If the change in wind direction with height is minimal, the wind direction will be parallel to and can be esti-

mated from the orientation of the cirrus blowoff (cirrus plumes). However, this procedure should not be used in an environment of strong vertical wind shear.

In an analysis of an outbreak of severe weather over the midwestern United States on May 5, 1971, Anderson [74] pointed out that "the threat tracks of the tornado producing storms are all oriented at a far greater angle to the right of the low-level flow than those of the non-tornado producers", which "indicates that the tornado-producing thunderstorms were all cyclonically rotating, right deviating severe storms." Burgess and Brown [73], in an analysis of Doppler radar data from a right moving thunderstorm, observed that the right moving cell (referred to as the Davis storm) possessed all of the radar supercell characteristics. "At least five short-lived tornadoes occurred" in the Davis storm area.

2.11. Low-Level Vorticity

Positive low-level vorticity and mid-level positive vorticity advection are indicative of severe weather which produces tornadoes. Vorticity is a vector quantity Ω which measures rotation. If Ω_x, Ω_y, and Ω_z are the components of Ω and u,v, and w are the components of the velocity vector V with respect to axes x,y,z, which are fixed in the earth, then the relative vorticity Ω_z is defined as below:

$$\Omega_z = \frac{\partial v}{\partial x} - \frac{\partial u}{\partial y}$$

The term vorticity (or relative vorticity) usually refers only to the vertical component Ω_z which measures spin in the horizontal plane. A parcel of air which rotates in the same sense as the Earth does in space is said to have positive, or cyclonic, vorticity. In order to compute vorticity "all

that need be measured is the velocity of the air. If this could be done with sufficient accuracy over a large area, it would be possible immediately to construct charts showing how the vorticity of the wind is distributed" (Sutton [61]).

Low-level cumulus clouds which exhibit cyclonic shear and curvature are indicative of positive low-level vorticity. Positive vorticity advection "can be identified where there is a small area of enhanced convective activity or, in certain cases, a formation in the shape of a comma" (Anderson [74]). "Cellular cloud patterns aid in the identification of..regions of positive vorticity advection." According to Clark [76] positive vorticity advecting over an area at mid-tropospheric levels can be "best defined on IR imagery as middle-level alto clouds as opposed to higher, colder cirrus clouds."

Positive low-level vorticity has been shown by Charba [76] to be correlated with the outbreak of tornadoes. Parmenter [76] observed from movie loops of visible SMS-2 imagery a low-level circulation with the comma pattern associated with rain/snow producing sub-synoptic systems around a large Gulf of Alaska low. The compact and well-defined nature of a vorticity comma cloud system, observed by Mathews and Johnston [76] was believed by the authors to imply "a concentration of positive vorticity advection (strong upward vertical motion), and thus [be]...indicative of the severity of this thunderstorm outbreak." The importance of mid-tropospheric vorticity advection in indicating waves on fronts which were associated with areas of heavy precipitation was illustrated in an analysis of frontal cloud systems by Parmenter and Anderson [74].

2.12. Upper-Level Divergence and Low-Level Convergence

Convergence and divergence refer to the accumulation and depletion (respectively) of mass in a volume of fluid. Low-level horizontal convergence implies that air is crowded into a smaller horizontal area and, since it cannot accumulate there, is forced to move upwards. As the air ascends, it cools adiabatically and condenses its water vapor into clouds, rain, and snow. Except in small-scale disturbances such as tornadoes, the rate of change of pressure at the surface is small ("barometric tendency") which means that the total divergence in a column of air must be small. Therefore, in order to "balance a large convergence of air in the lower levels of a cyclone, there must be a slightly greater divergence aloft" (Sutton [61]).

The mathematical term "divergence" includes both the meteorological concepts of convergence and divergence. If u,v, and w are the components of the velocity vector V in a coordinate system with axes x,y, and z, then the horizontal divergence of V is defined as

$$\mathrm{div}_H\, V = \frac{\partial u}{\partial x} + \frac{\partial v}{\partial y} \quad ,$$

For positive $\mathrm{div}_H\, V$, divergence is said to occur and for negative $\mathrm{div}_H\, V$, convergence.

The presence of convergence or divergence is, in practice, often estimated from the confluence or diffluence of the streamlines. Areas of convergence may appear in satellite imagery as very fine, closely spaced cloud bands (Holroyd [71]). Interpretations of cellular cloud patterns may enable the meteorologist to identify divergent flow in the cold air behind polar fronts over oceanic areas (Anderson [74]).

Auvine and Sikdar [73] pointed out that "divergence in the upper atmosphere gives a general indication of the region of upward motion." They con-

cluded that "fields of divergence and relative vorticity obtained from the (wind) vectors exhibit a consistent pattern with reference to the location of the jet axis and thunderstorm precipitation area". They noticed, however, that although the precipitation area was associated with an area of divergence, the location of maximum divergence did not coincide exactly with the location of the severe storm precipitation area. Among the features observed by Scofield [75] when tracking an upper air disturbance which produced heavy snowstorms were positive vorticity advection and upper air divergence.

Storms are often reported in the area of convergence of land, ocean, and sea breezes. A discussion of a variety of factors which influence the development of the sea breeze can be found in Purdom [74]. Local areas of convergence of the sea breeze lead to a strengthening of the cumulus activity along the sea breeze front with thunderstorms often forming along the merging of convective lines such as those resulting from two sea breeze fronts (for example, see Purdom [74] and Scofield and Weiss [76]). The convergence of the daytime winds blowing from the sea and the Gulf toward the Florida peninsula was one of the factors suggested by Edinger [67] which accounted for Florida's summer thunderstorms.

2.13. Speed-of-Cell Movement

An important feature for estimation of the severity of windstorms is the speed-of-cell movement. Displacements can be measured from pairs of enhanced infrared images using systems such as the ISI (Interpretation Systems Incorporated, Model #150) available at NESS (National Environmental Satellite Service) by locating the intersection of two cursors over the initial and final positions of the cell. Displacement of arc clouds which represented the leading edge of a gust front was compared by Gurka [76] with low-level wind speed. The results of the analysis revealed that "rapidly moving arcs

are generally associated with strong low-level winds".

2.14. Merging Cells

Investigations by Simpson and Woodley [71] indicate that merging cumulonimbus cells "often produce more than an order of magnitude more rain than isolated clouds on the same day, probably owing to dynamic invigoration of the merged cloud circulations". The authors suggested that "merger and organization are probably the first necessary steps in the formation of squall lines, tropical storm rainbands, and the giant cumulonimbus systems that fuel the large-scale equatorial air motions". Procedures for increasing the estimate of convective rainfall based on occurrence of merging thunderstorm cells were incorporated into Scofield's model for convective rainfall estimation (Fig.1). The merger of thunderstorm cells can be clearly seen in sequences of enhanced infrared images. Merger can also be detected in sequences of high-resolution visible imagery.

2.15. Splitting Cells

Splitting cells and right (or left) deviating storms are two severe storm features which usually occur together. A cumulonimbus cell is split into two separate sections when one of its members is rotating. The cyclonically rotating member moves to the right (right deviating storm) and tends to be tornadic. The right moving, tornado producing Davis storm studied by Burgess and Brown [73] resulted from the splitting on April 19, 1972, of an isolated thunderstorm over Western Oklahoma. After the split, the left moving section traveled 22 degrees to the left of the mean tropospheric wind while the Davis storm (the right moving section) traveled 25 degrees to the right of the mean wind. Figures 5-E-6 (i through l) of Anderson [74] illustrate the correspondence between splitting cells and tornado threat areas in both radar data and visible satellite data. Splitting cells can also be observed in sequences of enhanced infrared imagery.

3. Algorithms for Automatic Detection and Tracking of Severe Storm Features

The algorithms presented in this section address the four major problem areas below:

1) cloud classification
2) cloud segmentation
3) cloud geometry
4) cloud tracking

A review of algorithms applicable to the above topics and suggestions for future algorithmic development are included in this section. Cloud classification is the first step in identification of severe storm features. In order to determine wind fields, clouds must be classified into height categories. A description of cloud type is implicit in the nomenclature itself of some of the severe storm features. Low-level cumulus cloud line feeder bands consist of clouds of cumulus cloud type. Merging cells, splitting cells, etc., are features of *cumulonimbus clouds*. Positive vorticity centers are best defined as middle-level alto clouds (Clark [76]). When using GOES imagery in severe weather forecasting, observing cloud types and their change with time is used to infer changes in thermodynamic instability (Purdom [76b]). If cloud classification systems classify on an area basis instead of a point-by-point basis, cloud-segmentation techniques must be applied to obtain an outline of cloud features. The cloud segmentation of an area of satellite imagery can be partial (looking only for cloud features of a desired cloud type and shape) or total. If the cloud segmentation algorithms result in outlining and labeling cloud objects by cloud type only, shape properties (such as comma-tail, arc-shaped, line-shaped) must be determined by algorithms designed to characterize the geometrical properties of the segmented cloud objects. To detect on-going changes in shape and/or motion, cloud objects must be tracked from frame to frame.

3.1. Cloud Classification

A brief survey of cloud classification studies is followed in Sections 3.1.1. and 3.1.2. by a more comprehensive discussion of major cloud classification studies arranged within each section in chronological order. Methods to discriminate clouds from clear areas are presented in Section 3.1.1. The development of automatic cloud-type classification systems is reviewed in Section 3.1.2.

The problem of distinguishing clouds from clear areas was approached either from the standpoint of selection of appropriate thresholds or weighting functions. Arking [64], Katz [64], and Stamm and Vonder Haar [70] investigated methods for selection of a single threshold from visible measurements. These methods included manual selection of thresholds from series of thresholded images and/or comparisons of line plots of relative radiance vs. sample number and automatic selection of thresholds from gradient images and histograms of visible data within a grid area. Shenk and Salomonson [71] explored the effect of varying the ratio R of areal-cloud-size-to-areal resolution element on estimates of actual cloud cover. They concluded that the value of R must be at least 100 if cloud-cover estimates obtained by single-threshold methods were to be valid. Both Shenk and Salomonson [71] and Miller and Feddes [71] designed multiple threshold methods using weighting functions to estimate percentage of cloud cover.

Most of the cloud classification studies were conducted using cloud-type information over oceans. Over the oceans, the clear area is, in general, homogeneous; radiance spread is less than over land and difference in radiance levels between ocean and clouds is greater than that between land and clouds.

Threshold selection techniques to determine sea-surface temperature were developed by Smith et al. [70], Smith and Rao [72], and Leese et al. [71]. In tropical oceanic areas, either the sea-surface temperature (or a linear function of the sea-surface temperature) could be used to discriminate clouds from background. The linear function used by Koffler et al. [73] to separate clouds from clear area was T - 5°C, where T was the sea-surface temperature for the given grid area.

Cloud-type classification systems using only visible data characterized cloud types by form, pattern, texture, and dimensions or layers of the patterns and forms. The guides to interpretation of TIROS satellite pictures prepared by Conover [62] motivated several of the earlier studies. Rosenfeld [65] determined optimal window sizes for discrimination of cloud patterns into categories such as "brokenness", elongation, fibrosity, and convexity. Leese [64] used statistical methods to determine synoptic-scale features for classifying low-level cumuliform cloud patterns which occur over the oceans by cloud amount, size of the cumuliform cells, and size of the cloud bands. Cell size was found to be related to the location of the observation and the wind velocity field. Cloud amount was related to the location of the observation with reference to the center of the anticyclone, to the latent heat transfer between the ocean surface and the atmosphere, to the wind fields at the surface and at the 850 mb level, and to the air-dewpoint temperature difference at the surface. Surface wind speed was also an important factor in discriminating among groups of cloud bands. Katz derived motion-invariant features based on the autocorrelation function to measure the direction and the degree of alignment of cloud streets. Darling and Joseph [68] tested seven different pattern recognition techniques for discrimination of noncumulus clouds from cumulus

clouds and solid cell cumulus clouds from polygonal cell cumulus clouds. The screening multiple regression technique with four or fewer discriminators performed as well on independent samples as other techniques which used 300 to 400 properties. Booth [72] used multiple discriminant analysis techniques and perceptron training methods to isolate single-layered, low-level cloud regions. In order to resolve ambiguities between cloud classes, the author recommended the addition of infrared features to the pattern vector.

With the availability of multispectral satellite data, automatic systems for discrimination of cloud types (as opposed to cloud forms or shapes) were developed. Koffler et al. [73] used NMC (National Meteorological Center) temperature values to classify clouds by height. Greaves and Chang [70] determined cloud-type signatures from design samples of NIMBUS-2 cloud data over the continental United States in which there was relatively uniform cloud cover and no rapid clearing or buildup. The point-by-point classification method of Greaves and Chang [70] successfully identified all cloud types except for cumulus and cumulonimbus. The lack of success for cumulus-type clouds was attributed to the nonhomogeneous nature of the cloud field. A combination of thresholds derived from a radiative transfer model, climatological knowledge of the upper boundaries of cloud-type surfaces for a given area, and expected reflectance values for cloud types was used by Shenk and Holub [72] and Shenk et al. [76] to establish four-channel cloud-type signatures for cloud types over tropical oceans. Booth [73] combined statistical pattern recognition techniques with feature extraction methods to classify high-resolution, dual-channel NOAA-1 cloud samples over tropical oceanic regions. A comparative study of selected feature sets and statistical pattern recognition techniques to classify tropical oceanic-cloud types was conducted by Parikh [77a]. Classification

accuracy deteriorated depending on the complexity of the cloud-type decision problem. Optimal thresholds, either for point-by-point cloud-type signatures or for decision regions in feature vector space, did not remain constant with change in location or season of observation. A method of cloud classification by cloud-sample segmentation and comparison of segment features was developed by Parikh [77b]. The method was independent of design samples or prior threshold selection techniques. All of the above multispectral techniques except for that of Greaves and Chang [70] have been tested primarily or exclusively on cloud data over oceanic regions. Further study is needed to determine what modifications must be made either in cloud-type signature classification systems or feature-extraction classification systems to discriminate cloud types over land.

3.1.1. Methods for Distinguishing Clouds From Clear Areas

The earliest attempts to separate clouds from background involved finding a brightness threshold c such that all points with brightness values above c were designated as clouds and points with brightness values equal to or less than c were designated as background. Except for snow- or ice-covered regions, regions of thin cirrus, or regions of small and scattered convective cloud elements below sensor resolution size, a brightness threshold should be a good criterion for the detection of the presence of clouds against a dark background such as the ocean surface. According to Stamm and Vonder Haar [70], a histogram of the frequency at which a given radiance level occurs within a grid area will contain a peak of roughly Gaussian shape representing a clear area provided the clear area is homogeneous (ocean surface rather than land surface). However, even for ocean surfaces it is difficult to determine the point to the right of the Gaussian clear-area peak at which cloud interference is becoming important.

Limitations of sensor systems as well as variable brightness responses for a cloud of given reflectivity must be considered for both manual and automatic estimates of

cloud cover. Thin cirrus is transparent or semitransparent and the reflectance characteristics of the underlying background determine the recorded brightness intensity level. Small cumulus clouds below resolution size cannot be seen on the image but their brightness affects the sensor reading. Variabilities of the signal within a camera system, changes of response from one system to another, weakness in the cross track normalization technique, changes in camera calibration and degradation in camera response substantially alter the brightness response of individual cloud elements from day to day.

In 1964, Arking [64] discussed the problem of cloud/background threshold selection in connection with automatic analysis of Tiros III television pictures to determine latitudinal distribution of cloud cover. Arking's approach was to employ the subjective judgment of a human observer to compare a series of two-level thresholded images to the original satellite image to determine which of the thresholded images most faithfully reproduced the cloud boundaries of the original image. For each orbital sequence a new threshold was chosen. It was found, however, that the same threshold could be used for each satellite picture within a given orbit.

Katz [64] constructed a gradient image to automatically

determine a brightness threshold. The gradient image is defined as the image whose value at every point is given by

$$|| G || = \sqrt{(\partial I/\partial x)^2 + (\partial I/\partial y)^2}$$

where I is the brightness value of the given point. $|| G ||$ can be approximated by $|| \bar{G} ||$ where

$$|| \bar{G} || = \max\{|\partial I/\partial x|, |\partial I/\partial y|\} + \frac{1}{2} \min\{|\partial I/\partial x|, |\partial I/\partial y|\}.$$

In order to facilitate handling the pictorial data in packed form, the quantity actually used for computation of the gradient image was $2\,||\bar{G}||$. The cumulative frequency percentile was calculated for each gradient level in the gradient image. The smallest gradient level g for which the cumulative frequency percentile was greater than or equal to a given value p was then selected. Experimental results were calculated for p = 75%, p = 87.5%, and p = 93.7% with the value of p = 87.5% the personal choice of the author. The average intensity of those points at which the gradient was at least g was used as the threshold for cloud/background separation.

Shenk and Salomonson [71] suggested using two brightness thresholds to divide the satellite image into three data sets -- data where the resolution element is clear, data where the resolution element is partially cloud filled, and data where the resolution element is completely cloud filled. Let N_1 be the number of points in the first data set, N_2 the number of points in the second data set, and N_3 the number of

points in the third data set. Then the percentage N_c of cloud cover was calculated as

$$N_c = \frac{N_2+2N_3}{2(N_1+N_2+N_3)}$$

The association of a weight of 1 with elements in the second data set and a weight of 2 with elements in the third data set implies that a cloud cover of 50% is assumed for every partially cloud-filled resolution element. This two-threshold method is contrasted with the single-threshold method which divides a satellite image into points where the resolution element is clear and points where the resolution element is partially or completely cloud filled. For a typical situation in the tropics in which the average cumuliform cloud size is 4 km and for a typical sensor resolution of 4 km, the single-threshold method would estimate a true cloud cover of 20% as 70% cloud cover. The authors concluded from studies on simulated data and high-spatial resolution (300 feet) Apollo 6 photographs that the value of the ratio R of areal cloud size to areal-resolution element must be at least 100 if cloud cover estimated from single-threshold methods and actual cloud cover are to agree within approximately 10%. However, if cloud cover is estimated by the two-threshold method, good cloud cover estimates result for values $R \geq 10$. If the value of R is known, nomograms presented by the authors can be used to obtain true cloud cover from estimated cloud cover.

The question of automatic selection of the one or two brightness thresholds did not arise in the study of Shenk and

Salomonson [71]. The single-threshold method applied to simulated and high-resolution cloud data involved counting manually for each of seven resolution sizes the number of resolution elements which contained no cloud elements. Similarly, for the two-threshold method, a manual count was made of those resolution elements which were partially cloud filled and of those which were completely cloud filled.

Automation of a multiple threshold, weighted histogram model for cloud-cover estimation was described by Miller [71] and Miller and Feddes [71]. Satellite image data compressed from a 0-63 scale to a 0-14 scale was divided into the five equally-spaced brightness ranges 0-2, 3-5, 6-8, 9-11, and 12-14. With each brightness range was associated an empirically-derived seasonal weight. For October-May, the weights W_i, $i = 1,\ldots,5$, for the five brightness ranges were 0, 2, 7, 8, 8, respectively. For June-September, the weights W_i, $i = 1,\ldots,5$, for the five brightness ranges were 0, 2.5, 7.5, 8, 8, respectively. Higher weighting of classes 2 and 3 for the summer months reflected the increased frequency of occurrence of small cumulus cloudiness during the summer. The percentage N_c of cloud cover was calculated as

$$N_c = \left(\frac{\sum_{i=1}^{5} W_i F_i}{64} \right) + k$$

where

W_i = weighting factor for class i

F_i = frequency of occurrence of the ith class

k = 0.51, a computer truncation constant.

The N_c values, although in general agreement with concurrent surface observations, showed a consistent tendency to underestimate surface reports of cloud cover. Miller and Feddes [71] ascribed the differences primarily to differences between the field of view of the surface observer and the angle of view of the satellite camera (which resulted in an overestimate of cloud cover from surface observations) and to the lower response threshold (i.e., lack of sensitivity to thin cirrus or to small, scattered convective elements) and resolving power of the satellite sensor. The authors concluded that the automated values for N_c were at least as good as those which could be derived by eye from satellite pictures.

A threshold $\overline{T}$ can be applied to infrared measurements of cloud data to discriminate clouds from background. Over the oceans, an appropriate value for $\overline{T}$ for each grid area of the image would be either the sea surface temperature T within that grid area or T-k where k is some small positive constant. Koffler et al. [73] subtracted a constant of 5°C from the sea surface temperature to determine the grid area thresholds $\overline{T}$. All grid points with infrared temperature greater than or equal to $\overline{T}$ were classified as background points.

A statistical histogram method to determine the sea surface temperature values T from nighttime 3.8 μm infrared data is given in Smith et al. [70]. The following procedure was used to analyze the temperature histogram. If a clear distribution (Gaussian) could be detected such that the maximum frequency of a point of the clear distribution was both at a temperature

greater than freezing (273°k) and greater than 10 percent of the total number of observations, then the histogram was considered to be sufficiently cloud free to be acceptable for the second stage of analysis. Find the point M_{slope} on the high temperature wing of the clear distribution where the change of frequency with temperature is a maximum,i.e., the point of maximum slope. Define M_{high} as the highest observed temperature value with a frequency greater than 1 percent of the total number of observations. Define T as

$$T \equiv M_{slope} - \sigma$$

where

$\sigma \equiv$ known standard error of measurement

For this study (Nimbus 2), $\sigma = 1.5°K$. T will usually be greater than the modal peak temperature of the clear distribution when clouds exist. If the difference between M_{high} and T is greater than 3σ or if the change of frequency with temperature at M_{slope} is less than 3 percent per degree K, then the high temperature wing of the clear distribution is influenced by cloud-contaminated measurements and sea-surface temperature cannot be specified. Otherwise, specify the sea-surface temperature as T.

Sea-surface temperatures for areas of severe cloud contamination were inferred through space and time interpolation procedures. In a few cases in which the histogram technique failed to differentiate between cloud-free and cloud-contaminated temperatures, errors were attributed to the existence of low-level, uniform, overcast conditions.

The authors suggested using either spatial gradient consistency checks and/or time compositing techniques to filter out erroneous sea temperatures. Relative discrepancies between the histogram sea-surface temperatures and ship-reported sea-surface temperatures were generally less than 1°K.

Smith and Rao [72] developed an algorithm to determine both daytime and nighttime sea-surface temperatures from spatially contiguous sets of simultaneous 3.7μm and 11μm infrared measurements. The contiguous resolution elements were assumed to have the same average cloud temperature and sea-surface temperature, i.e., the same type of cloudiness conditions. For resolution elements 1 and 2 and spectral windows 3.7 μm and 11 μm, the ratio of the cloud amounts of the two resolution elements were equated for each spectral window, i.e.,

$$\frac{I^1_{3.7} - B_{3.7}(T_S)}{I^2_{3.7} - B_{3.7}(T_S)} = \frac{I^1_{11} - B_{11}(T_S)}{I^2_{11} - B_{11}(T_S)}$$

where

I^r_S = measured radiance for resolution element r for spectral wavenumber S

$B_S(T_S)$ = Planck radiance for spectral wavenumber S

The Planck radiance $B_S(T)$ is a function of temperature which is given by

$$B_S(T) = C_1 S^3 / (\mathrm{EXP}(C_2 S/T) - 1)$$

where

$$C_1 = 1.19061 \times 10^{-5} \text{ erg-cm}^2\text{-sec}^{-1}$$

$$C_2 = 1.43868 \text{ cm-deg}$$

If the relation R(T) is used to denote the result of equating the ratio of cloud amounts for the two spectral windows, i.e., $R(T) \equiv I^1_{3.7}I^2_{11} - I^2_{3.7}I^1_{11} + B_{11}(T)[I^2_{3.7} - I^1_{3.7}] - B_{3.7}(T)[I^2_{11} - I^1_{11}]$, then we can solve for T_S (sea-surface temperature) by setting $R(T) = 0$. The first order Taylor approximation for T (where the superscript k denotes a quantity evaulated for the kth iteration) is given by

$$T^{k+1} = T^k - [R^k / (\frac{\partial R}{\partial T})^k]$$

where

$$(\frac{\partial R}{\partial T})^k = [I^2_{3.7} - I^1_{3.7}](\frac{\partial B_{11}}{\partial T})^k - [I^2_{11} - I^1_{11}](\frac{\partial B_{3.7}}{\partial T})^k$$

With an intial guess temperature of 310°k, a solution was usually obtained in less than five iterations. This multi-spectral approach was one method used by Smith to resolve the problems of interpretation of daytime 3.7 μm data in which cloud contaminated temperatures can be equal to or larger than clear sky brightness temperatures.

Another approach suggested by Smith for determining sea-surface temperatures using single-channel data was described in a paper by Leese et al. [71]. This method assumed a Gaussian distribution of the system noise, but unlike the method of Smith et al. [70] previously reviewed, the value σ of the standard error of measurement (noise) was not assumed to be known. Given any three temperature classes of the

clear distribution, the sea-surface temperature T_S which is the mean value of the distribution from clear atmosphere samples was computed as

$$T_S = \frac{(T_3^2 - T_1^2)\ln F_1/F_2 + (T_1^2 - T_2^2)\ln F_1/F_3}{2(T_1 - T_2)\ln F_1/F_3 - 2(T_1 - T_3)\ln F_1/F_2}$$

where

T_i, i = 1, 2, 3 is the ith temperature class

F_i, i = 1, 2, 3 is the frequency of occurrence of temperature class T_i.

A distribution of values of T_S was obtained by using a number of combinations of temperature classes taken three at a time. The mean value of this second distribution was used as an estimator for the sea-surface temperature T_S. Six cloud and noise contamination tests had to be passed by the second distribution of values for T_S for the sample to be retained for sea-surface temperature calculations. Since cloud layers can produce histograms of the same shape as those obtained from a clear atmosphere, Leese suggested that instead of just restricting T_S to be above 273°k, a suitable test should be developed on the basis of first-guess fields. A first-guess field for the sea-surface temperature value could, for example, consist of the previous day's temperature combined with appropriate limits for acceptable twenty-four hour changes (obtained from gradient calculations). Results indicated that errors of less than 1°C should be possible for areas where the temperature gradient is less than 2°C per

100 km. For regions where the temperature gradient was 2 to 4°C per 100 km, visual data should be included to reduce cloud contamination errors. Improvements may be needed in earth location procedures if an error of less than 1°C is to be maintained for regions in which the temperature gradient is larger than 4°C per 100 km.

Stamm and Vonder Haar [70] suggested as a result of threshold studies in the visible channel that some combination of threshold criteria in several spectral channels would be able to detect cloud contamination with better precision than single-channel thresholds. They investigated two threshold methods for the visible channel. The first method compared a line plot of relative radiance vs. sample number to a corresponding line on the given picture to manually determine a threshold between cloud and background regions. The second method analyzed the histograms of radiance levels within a given grid. For grid areas over oceans with a reasonable amount of clear area, a large peak of roughly Gaussian shape represented the clear area. By forming a Gaussian curve from the data on the left-hand side of the peak (the side free from cloud interference), it was possible to predict the clear area peak. The point at which the Gaussian curve starts to rise again, or a few radiance levels to the cloudy (right) side of this clear area peak, was chosen as the threshold. When in doubt, the threshold was chosen to overestimate the cloudy regions.

3.1.2. Automatic Cloud-Type Classification Systems

Various automatic cloud classification systems using features derived from visual satellite data, infrared satellite data, and multispectral satellite data have been developed from 1964 to the present date. In this section, a brief survey of techniques and results of single-channel cloud classification systems is followed by a more comprehensive review of multispectral systems.

Conover [62] published in 1962 a guide to cloud interpretation from satellite pictures. Features selected to discriminate cloud types were form (round, curved, or elliptical), pattern (banded or randomly spaced), texture (smooth versus fibrous), brightness, structure, and dimensions of the patterns and forms. Each cloud type was associated with one of four brightness classes -- dark gray, gray, white, and very white. The author suggested use of automatic methods for cloud reflectivity contouring as an aid to photointerpretation of satellite images. The idea of characterizing cloud types by ranges of measurements in one spectral window was a forerunner to completely automated cloud-type classification schemes such as that of Shenk and Holub [72] in which ranges of measurements in four spectral windows specified a

unique cloud type.

In 1964, Leese [64] applied multiple-discriminant analysis techniques to the problem of classifying low-level cumuliform cloud patterns by cloud amount, size of the cumuliform cells, and size of the cloud bands. Twenty-three synoptic features consisting of variables such as latitude, longitude, mean solar time, surface-geostrophic wind speed, and latent heat flux were used to categorize the cloud patterns into cloud cover groups, cloud size groups, and cloud banding groups. Cloud amount was found to be most closely related to the location of the observation with reference to the center of the anticyclone. Size of the cumulus cells was most closely related to the structure of the wind field between the 850-mb level and the surface. Discrimination results between cloud banding groups were not as successful as discrimination results between cloud amount groups and cloud size groups. More objective techniques for the original description of the cloud patterns (such as increased number of cloud amount groups, information on cloud patterns on different size scales, and a coordinate system to describe the location of the observation in the anticyclone) combined with improvements in the sensor system of the satellite were suggested as possible factors which would improve classification results. In particular, two-dimensional spectral analysis techniques such as numerical filtering should be used to provide information about cloud patterns on at least three scales -- the synoptic scale

(more than 50 mi), the mesoscale (between 10 and 50 mi), and the submesoscale (less than 10 mi).

Rosenfeld [65] discussed a scanning window approach to automatic classification of cloud patterns into categories representing sparseness or "brokenness", fibrosity, elongation, regularity, straightness, and convexity properties. Quantitative measurement scales for these parameters were derived from psychological studies of human judgments of these parameters in a series of cloud photographs. In order to discriminate between solid black (background), solid white (cloud), and broken cloud regions, the number of background elements in the scanning square window of an image was counted for each position of the window. If the number of background elements fell below a threshold T_W, the square was called solid white. If the number of background elements was greater than a threshold T_B where $T_B \geq T_W$, the square was categorized as solid black. Otherwise, it was considered as broken cloud. Boundaries between regions of different types were marked. Suggested window sizes for discrimination of cloud patterns with respect to the above parameters were 5x5 resolution elements for "brokenness" and 15x15 resolution elements for shape and size properties.

Katz [64] derived motion-invariant features to describe the degree and direction of alignment of striated clouds and considered features which would give information about the distribution of cloud sizes in a region. The ratio of the axes of the ellipse of concentration of the central hump of the autocorrelation function $\rho(h,k)$ was used to measure the

degree of alignment of cloud streets. The direction of the major axis was taken to be the direction of the streets. The ellipse of concentration was taken as the contour enclosing the central hump of $\rho(h,k)$ for which $\rho(h,k) = 0.2$. The direction of the major axis of the ellipse was given by

$$\tan 2\theta = \frac{2\mu_{11}}{\mu_{20}-\mu_{02}}$$

where μ_{ij} are central moments. The ratio r of the axes is $r = \sqrt{\lambda_1/\lambda_2}$, where λ_1 and λ_2 are the roots of

$$(\mu_{20}\mu_{02}-\mu_{11}^2)\,\lambda^2 - (\mu_{02} + \mu_{20})\lambda + 1 = 0.$$

The autocorrelation function $\rho(h,k)$ is the normalized (divided by the individual variances) autocovariance function $C(h,k)$ where

$$C(h,k) = \iint [I(x,y)-m][I(x-h,y-k)-m]\,dxdy$$

with

$I(x,y)$ = brightness level at point (x,y)

m = mean value of I

The feature a(t) described by Blum [62] where a(t) is the area at time t of the region enclosed by a wavefront moving from a pattern at constant speed in all directions was proposed to characterize the distribution of cloud sizes. As the dark areas overrun the cloud areas, the clouds begin to disappear -- for a convex cloud, this would happen in the time it takes the wave to traverse half the width of the cloud.

Darling and Joseph [63] applied five linear decision

techniques, one nonlinear decision technique ("Madaline"), and a screening multiple regression technique to categorize cloud patterns into cumulus and noncumulus classes and to categorize cumulus clouds into cumulus polygonal cell patterns and cumulus solid cell patterns. For the linear decision function techniques and for Madaline, a group of n threshold units $b_i(j)$, $i = 1,\ldots,n$ were randomly connected to elements in the pattern space. The output of the ith logic unit $b_i(j)$ for the jth pattern is 1 if a function of its inputs exceeds a threshold and 0 otherwise. The threshold was defined by a quadratic switching surface

$$X^T(\Sigma_1^{-1}-\Sigma_2^{-1})X-2X^T(\Sigma_1^{-1}M_1-\Sigma_2^{-1}M_2)+M_1^T\Sigma_1^{-1}M_1-M_2^T\Sigma_2^{-1}M_2+\ln(|\Sigma_1|/|\Sigma_2|)=0$$

where vectors M_1 and M_2 are sample means and Σ_1 and Σ_2 are covariance matrices for classes 1 and 2 respectively and X is the pattern vector. The form of the decision function D(j) for the linear-decision techniques was

$$D(j) = \sum_{i=1}^{n} w_i b_i(j) - \theta$$

where

$w_i, i = 1,\ldots,n$ are property weights

θ is the response unit threshold

Weights and response function were calculated according to the following five algorithms -- forced learning, Bayes weights, error correction, iterative design, and mean square error. The first three methods are associated with the α perceptron of Rosenblatt. For Madaline, a second layer of threshold-logic units was connected between the first set and

the response unit (decision function).

For the screening multiple regression technique, twenty-eight features computed from a binary representation of the scene were screened at the 0.01 level. For this technique, the decision function was a linear multiple regression equation of the form

$$\hat{x}_0 = \lambda_1 x_1 + \lambda_2 x_2 + \cdots + \lambda_p x_p$$

where

$$x_0 = \begin{cases} n_2/(n_1+n_2) & \text{in class 1} \\ -n_1/(n_1+n_2) & \text{in class 2} \end{cases}$$

$\hat{x}_0$ is an estimate of x_0

n_i is the number of samples in class i

x_i is the deviation from the mean value calculated over both classes

λ_i's are constants to be determined by least squares.

At each step, the particular x_i having the highest correlation r_{0i} with x_0 is added to the equation if the reduction in variance r_{0i}^2 is greater than 0.01. The correlation r_{0i} is defined as

$$r_{0i} = d_i \sqrt{\frac{n_1 n_2}{S_{ii}(n_1+n_2)}}$$

where

d_i = difference between the mean value of x_i in class 1 and its mean value in class 2

S_{ii} = sum of squares of x_i over both classes.

The value of λ_i is given by

$$\lambda_i = \frac{d_i n_1 n_2}{s_{ii}(n_1+n_2)}$$

After the selection of each x_i, the remaining x_i's are orthogonalized with respect to the selected x_i to yield an equation for $\hat{x}_0$ with uncorrelated terms. The decision rule is: if $\hat{x}_0 > -\frac{1}{2}[(n_1-n_2)/(n_1+n_2)]$, assign the pattern to class 1. Otherwise, assign the pattern to class 2 if $\hat{x}_0 < -\frac{1}{2}[(n_1-n_2)/(n_1+n_2)]$. For the classification of non-cumulus versus cumulus clouds, the features chosen were the 80-contour area (area bounded by the Y axis and 0.80 autocorrelation contour for X > 0), the brightness variance, and the relative frequency of cloud size 1 to 25 (i.e., from 1 to 25 resolution elements).

Decision accuracies for the error correction procedure, iterative design, Madaline, and screening multiple regression techniques were close to 90%. The authors noted that the screening multiple regression technique with only three to four discriminators performed as well or better than the other techniques which used approximately 400 properties. They recommended enlarging the set of features to include information content in the derivative, curvature, gradient, and Laplacian of the brightness image, the coefficients of the power spectrum, and the characteristics of the autocorrelation function obtained by rotating a pattern about its center of gravity.

Booth [73] categorized 32x32 visual arrays of ATS-1 images into a 5-group model and a 3-group model using multiple

discriminant analysis and perception training methods. The 5-group model consisted of

(1) predominantly single-layered, low-level (≤ 8000 ft) cloud regions

(2) predominantly single-layered, middle- or single-layered high-level cloud regions

(3) predominantly multi-layered or large convective cloud regions

(4) cloud regions containing more than one of the above groups with one group not dominant

(5) none of the above (i.e., overcast and clear-sky cloud regions).

The 3-group model consisted of classes 1, 2, and 3 above. Results of multiple discriminant analysis using forty-six features assumed to be normally distributed with the same covariance matrices ranged from 68% decision accuracy for group 1 independent (test) data for the 5-group model to 92% decision accuracy for group 1 independent data for the 3-group model. Every misclassified group 1 sample was labelled as group 3 by the multiple discriminant classifier -- thus pointing out the confusion between groups 1 and 3. Tests on independent data were performed exclusively on observations from group 1, since the primary intent of this classification system was to isolate those regions which would be suitable input target areas for the automated operational system of NOAA for computation of single-layered, low-level wind vectors.

Experiments to separate group 1 from the combined groups 2 and 3 by perceptron analysis failed after 454 iterations. The similarities between groups 1 and 3 obviously led to the lack of linear separability between observations from group 1 and observations from groups 2 and 3. Perceptron classification of 787 test observations into cloud and no-cloud groups resulted in 653 (83%) observations correctly classified.

Suggestions by the author for improvement of decision accuracy were to

(1) construct a new 5-group model consisting of low-level single-layered regions, middle-high level single-layered regions, multi-layered or convective regions, overcast regions, and clear-sky regions,

(2) augment the pattern vector with features from infrared satellite data such as cloud-top temperature to help resolve ambiguities, for example, between groups 1 and 3, and

(3) generate an optimum input pattern vector by performing screening analysis on features derived from the satellite data.

Satellite infrared radiation (IR) temperatures segmented at each grid square (32x32 IR spots) into four intervals dependent on synoptic temperature fields obtained on a 12-hour basis from the National Meteorological Center (NMC) were used by Koffler et al.[73] to generate pictorial displays of cloud-type information consisting of four gray shades. Each of the four gray levels represented a cloud category as shown in

Table 2.1 below.

Gray Shade	Temperature Interval	Cloud Type	Cloud Top Height Interval
black	Infrared Temperature $\geq \overline{T}_1$-5°C	no clouds	———
dark gray	$\overline{T}_1$-5°C > Infrared Temperature > $\overline{T}_2$	low clouds	surface - 700 mb layer
light gray	$\overline{T}_2 \geq$ Infrared Temperature $\geq \overline{T}_3$	middle clouds	700 mb - 400 mb layer
white	$\overline{T}_3$ > Infrared Temperature	high clouds	above 400 mb layer

Table 2.1: Cloud classification system of Koffler et al. [73]. Threshold values $\overline{T}_1$, $\overline{T}_2$, $\overline{T}_3$ represent, respectively, NMC temperature values per grid area at the surface, 700 mb, and 400 mb.

Assumptions inherent in the use of this classification scheme are:

(1) clouds are completely opaque,

(2) radiation emanates from cloud tops,

(3) there are no rapid atmospheric changes in the time interval between the NMC data and the infrared temperature data,

(4) the earth's actual surface temperature is constant over the area of a grid square and equivalent to the NMC-supplied earth surface temperature, and

(5) errors caused by assignment of an IR temperature measurement to the lowest pressure layer in cases of a non-unique correspondence of a particular IR temperature to a given pressure interval resulting from the existence of an isothermal or near-isothermal atmosphere or from the existence of inversions, are minimal.

Assumption number (1) leads to errors of interpretation especially in the case of cirriform clouds. For cirrus clouds with an ice concentration of 0.01 $g \cdot m^{-3}$ a thickness of almost 5 km is required to assure that the assumption of opaqueness is reasonably satisfied. Thin trailing edges of cirrus which generally exhibit low emissivity may be classified, for example, in the 700-400 mb layer rather than the layer above 400 mb. For this reason, it is suggested by Koffler et al. [73] that the cloud data be interpreted as lying above 700 mb rather than exactly within the 700-400 mb layer. If assumption number (4) is not valid over a given NMC grid area (12 km at 45°N), then there will be errors in the calculation of the amount of low cloud. To insure that earth surface view is not included as low clouds, a factor of 5°C is subtracted from the surface temperature $\overline{T}_1$ supplied by NMC.

Results obtained by Koffler et al. [73] show good large-scale agreement with surface observations and pilot reports while offering the advantage of greater geographical coverage. The authors state that "problems and errors of the

system are probably no greater than that of the surface observation system." There is however a tendency to overestimate cloud amount and underestimate the temperature of cloud top heights as a result of satellite sensor resolution. If the size of a cloud element is near or below the sensor resolution, the IR temperature spot will represent a combination of the temperature of the surface and the temperature of the cloud, thus causing the entire area to be classified as cloud with the cloud top height placed at lower than actual level. This type of error can be expected over areas of fair weather cumulus typical of oceanic regions. The given classification system can be applied over oceanic regions in the Southern Hemisphere where NMC data is not available by using vertical temperature profiles determined from sea-surface temperature estimates generated from satellite IR data as described in Rao [70].

Historically one of the first attempts at multispectral cloud-type identification was the work of Greaves and Chang [70] which included

(1) an analysis of the statistical distributions of five cloud types using three-channel radiometric data at spectral intervals .2-4.0 μm, 6.4-6.9 μm, and 10-11 μm,

(2) derivation of cloud signatures from mean and standard deviations observed in the reflectance channel (.2-4.0 μm) and the temperature channel (10-11 μm),

(3) implementation and testing of a decision system

based on rectangular decision regions, and

(4) formal development of a decision matrix system for elliptical decision regions.

Data from Nimbus II at places where a relatively uniform cloud cover was reported over a large area, where there was no rapid clearing or buildup of clouds, and where ground-observed documentation of cloud type and cloud cover was available were divided into a test set and a design set which was used for development of cloud-type signatures for five different cloud types categorized as follows:

(1) cumulus

(2) stratus and/or stratocumulus

(3) altocumulus

(4) cirrus

(5) cumulonimbus.

An analysis of the statistical distributions of each cloud type in each of the three radiometric channels revealed that while the distributions in the reflectance and temperature channels exhibited characteristic maxima and spreads per cloud type, the information content of distributions in the water vapor channel (6.4-6.9 μm) was low in terms of cloud-type differentiation. A primary advantage of incorporating temperature data from the water-vapor channel into a given classification scheme was the fact that cloud data could easily be separated from clear skies by classifying all points as clear in which the temperature obtained from the water-vapor channel was greater than 240°K. This threshold

proved adequate even in identification of tenuous cirrus as cloud data. With the assumption that the distributions are approximately Gaussian, mean and standard deviations for the five cloud types in the reflectance and temperature channels were computed as shown in Table 2.2 below.

Cloud Type	$\overline{T}$	$\sigma(\overline{T})$	$\overline{R}$	$\sigma(\overline{R})$
cumulus	274°K	4.8°K	0.21	0.06
stratus/stratocumulus	281°K	2.8°K	0.59	0.06
altocumulus	262°K	5.0°K	0.54	0.08
cirrus	295°K	3.6°K	0.10	0.03
cumulonimbus	224°K	6.4°K	0.62	0.09

Table 2.2: Cloud-type signatures used by Greaves and Chang [30].

$\overline{T}$ represents mean temperature in the spectral interval 10-11 μm

$\sigma(\overline{T})$ represents standard deviation in the spectral interval 10-11 μm

$\overline{R}$ represents mean reflectance in the spectral interval .2-4.0 μm

$\sigma(\overline{R})$ represents standard deviation in the spectral interval .2-4.0 μm

It should be noted that the relatively high value of $\overline{T}$ for cirrus is a result of transmission to the satellite of radiation from lower levels. The standard deviation $\sigma(\overline{T})$ which

represents the degree of nonuniformity in cloud-top height or cloud thickness is seen to be maximal for cumulonimbus observations.

A given data point with reflectance R and temperature T was classified as belonging to cloud type i if

$$|R - \bar{R}_i| \leq K\, \sigma(R_i)$$

and

$$|T - \bar{T}_i| \leq K\, \sigma(T_i)$$

where $\bar{R}_i$, $\bar{T}_i$, $\sigma(R_i)$, $\sigma(T_i)$ are values given in Table 2 above and K is a range factor chosen as K = 2.5 for the given implementation. The authors suggest that the optimum value of K for classification of most data points without excessive overlap between cloud types lies between 2.0 and 2.5. In cases where a data point fell into overlapping regions of two different cloud types, it was considered to be correctly classified if either of the cloud types corresponded to the ground-truth identification (which was based on data from ground observations as well as analysis of satellite photographs).

The percentage of correctly classified data points per cloud type were as follows:

(1) 43% for cumulus

(2) 78% for stratus/stratocumulus

(3) 72% for altocumulus

(4) 80% for cirrus

(5) 34% for cumulonimbus

The authors attribute the lack of success in point-by-point identification of cumulus and cumulonimbus to the nonhomogen-

eous nature of these cloud fields and attribute the high degree of success in recognition of the remaining cloud types partially to the fact that the test samples consisted only of regions identified as being covered by a single type of cloudiness. They suggest that spatial frequencies be considered to facilitate the identification of cumuliform cloud types.

A decision matrix approach to cloud classification using elliptical boundaries was formulated for a 2-group cloud-type model as follows: Store in the computer memory a 20x20 decision matrix D where the value of the decision matrix at D(r,t)[where r is the rth reflectance interval (with each of 20 intervals representing a 5% increment in reflectance) and t is the t^{th} temperature interval (with each of 20 intervals representing a 5% increment in temperature)] can assume any of the values 0, 1, 2, 3 which stand for the four possible classifications

0 - no decision

1 - cloud type 1

2 - cloud type 2

3 - ambiguous between cloud types 1 and 2

The value assigned to element D(r,t) of matrix D depends on whether or not

$$\left[\frac{R-\bar{R}_i}{\sigma(\bar{R}_i)}\right]^2 + \left[\frac{T-\bar{T}_i}{\sigma(\bar{T}_i)}\right]^2 \leq N^2$$

where N^2 is a range factor (similar to the factor K above),

$R = 5r$

$T = 5t + 200°$

$\bar{R}_i$, $\sigma(\bar{R}_i)$, $\bar{T}_i$, $\sigma(\bar{T}_i)$ represent cloud-type signatures similar to those in Table 2 above.

If the above inequality is satisfied for both group 1 (i=1) and group 2 (i=2), then the value of D(r,t) is 3 which means that the classification is ambiguous. Once the decision matrix is stored in the computer, the classification of any data point is achieved by computing r and t from the reflectance R and temperature T and then consulting the entry D(r,t) in the decision matrix for the corresponding classification. The authors suggest the decision matrix approach for future configurations for cloud-type classification.

Shenk and Holub [72] proposed a multispectral cloud-type identification method based on a cloud-type decision matrix for the four spectral regions of 0.2-4.0 μm, 6.4-6.9 μm, 10-11 μm, and 20-23 μm. Decision categories were

(1) cirrus clouds
(2) cirrus with lower clouds
(3) cumulonimbus and/or cirrostratus
(4) cumulonimbus
(5) middle clouds
(6) middle clouds with cirrus above
(7) stratus or stratocumulus
(8) cumulus
(9) clear
(10) no decision

A data point from Nimbus 3 satellite imagery was classified into one of the categories 1-9 if measurements in all four spectral channel fell between the lower and upper threshold for that

particular cloud type. Otherwise, the data point fell into the no decision category. The authors recommended examining adjacent cloud decisions to obtain information on cloud conditions at "no decision" points.

Threshold values were calculated from a radiative transfer model which accepted as inputs average temperature and moisture sounds for the given test area during the study period, a climatological ozone profile, and cloud tops at different heights. It was assumed that low-cloud tops were at 750 mb, middle cloud tops at 450 mb, cirrus-cloud tops above 300 mb, and cumulonimbus-cloud tops below 225 mb.

From a total of 611 cloud-type decisions over a 30-mile swath covered by aircraft photographs, 85 decisions were misclassified. Two-thirds of the misclassifications represented a confusion between groups 1 and 2, which probably could have been avoided by different threshold choices for the visual channel. The remainder of the misclassifications except for two points were the result of labelling scattered low clouds or clear conditions as cirrus. Some of the misclassification errors were attributed to earth location errors in the satellite data, spatial resolutions, and time difference between aircraft and satellite observations. Modifications in cloud-type categories and cloud-type thresholds were later adopted (Shenk et al. [76]) which significantly improved classification accuracy.

Coincident infrared and visual data from NOAA-1 satellite were used by Booth [73] to test the discriminatory ability of

Bayesian and maximum-likelihood classifiers to separate 2100 cloud observations into a 6-group tropical cloud-type model consisting of

(1) clear skies

(2) cumulus

(3) stratocumulus

(4) cumulonimbus

(5) cirrus

(6) cirrus with lower clouds

and into a 5-group tropical cloud-type model obtained from the 6-group model by combining cumulus and stratocumulus into one group. A comparative study of the effect on each of the classifiers of selecting feature vectors from

(1) single-channel visual (.5-.7 μm) data

(2) single-channel infrared (10.5-12.5 μm) data

(3) dual-channel visual and infrared data

revealed that accuracy using single-channel infrared data approached that obtained by dual-channel classification.

A combination of features representing 32 spatial distribution measurements and 32 spatial frequency measurements were calculated for each 32x32 observation matrix (approximately 54x96 nmi.) of coincident visual and infrared data. The spatial distribution measurements selected for both IR and visual data were mean, standard deviation, coefficient of variation, skewness, kurtosis, range, mean-median, primary mode / secondary mode, average gradient, maximum quadrant coefficient of variation-minimum quadrant coefficient of varia-

tion, and cumulative frequency values at 1%, 16%, 50%, 84%, and 99% levels. The power spectrum measurements selected for both IR and visual data were values at wave numbers 1-11 and linear combinations of various wave numbers from 1-11. The spatial distribution measurements have typically been used to describe size, shape, and texture of cloud images. The power spectrum measurements denote the amount of variance in an observation due to clouds of various sizes. For example, given a grid size of 54x96 nmi., wave number 1 corresponds to a cloud size of 27x48 nmi.

Both the Bayesian and maximum-likelihood classifiers were designed on feature vectors obtained from 1050 observation matrices (half of the sample set) and were tested on both the design set (dependent data) and the remaining half of the sample set (independent data) not used for design. The conditional probabilities $p(i|\overline{X})$ where $p(i|\overline{X})$ is the posteriori probability that an observation belongs to group i given observation vector $\overline{X}$ were calculated under the assumptions that the feature vectors were normally distributed and that the covariance matrix of each class could be approximated by the pooled within-groups dispersion matrix $\sum_p$ where

$$\sum_p = \frac{(F_1-1)\sum_1+(F_2-1)\sum_2+\cdots+(F_k-1)\sum_k}{N-k}$$

where $\sum_i$ is the covariance matrix for group i, F_i is the group frequency for group i, N is the total number of observations, and k is the total number of groups. A priori probabilities P(i) for the Bayesian classifier were estimated from group-

relative frequencies obtained from the entire sample set (independent and dependent data). For the maximum-likelihood classifier all calculations were performed as for the Bayesian classifier with the exception that equal a priori probabilities were used. The decision rule was to classify and observation into group i if

$$P(i|\bar{X}) > P(j|\bar{X}) \quad \text{for all } j \neq i$$

where

$$P(i|\bar{X}) = \frac{P(\bar{X}|i) \cdot P(i)}{\sum_{i=1}^{k} P(\bar{X}|i) \cdot P(i)}$$

and

$$P(\bar{X}|i) = \frac{1}{(2\pi)^{n/2} |\sum_p|^{\frac{1}{2}}} \exp[-\frac{1}{2}(\bar{X}-\bar{M}_i)^T \sum_p^{-1} (\bar{X}-\bar{M}_i)]$$

with

$|\sum_p|$ defined as the determinant of the pooled dispersion matrix

k defined as the number of classification groups

M_i defined as the mean vector for the ith classification group

n defined as the number of features in feature vector $\bar{X}$.

With the threshold level for screening set at the 1% significance level, thirty-two features (sixteen from each channel) for dual-channel data, sixteen for single-channel IR data, and seventeen for single-channel visual data entered into the discriminant functions $g(\bar{X})_i$ (where $P(X|i) = \exp[g(\bar{X})_i]$)

calculated for the maximum-likelihood and Bayes classifiers using the stepwise multiple-discriminant analysis program (BMD07M) from the UCLA biomedical package. The feature which was the best single discriminator for dual-channel data was the IR value at the 1% cumulative-frequency level (at the cold end of the cumulative-frequency curve) which represents (for observations containing clouds) the temperature of cloud tops. For opaque clouds the thirty-two features chosen tend to measure various characteristics of cloud tops; however, for semi-transparent clouds such as cirriform the effects of underlying visual and infrared radiation contaminate the measurement of cloud-top characteristics. The minimum mean temperature ranges were found in stratocumulus samples. The maximum mean-temperature ranges were found in cumulonimbus and cirrus observations with the coldest mean temperature found in cumulonimbus observations. The mean temperature for cirrus observations was relatively high as a consequence of radiation transmitted from below the cloud tops. The maximum mean temperature gradient was found in cirrus observations. The feature which was the second best discriminator for dual-channel data was the visual value at the 99% cumulative frequency level which represents high albedo. Mean relative brightness was a maximum for cumulonimbus observations, a minimum for clear observations, relatively low for cumulus observations as a result of the nonhomogeneous nature of cumuliform clouds, and considerably higher for stratocumulus observations. Range in mean cloud brightness was maximum for

cumulonimbus and minimum for observations containing only cirriform clouds. The largest mean brightness gradients were found in cumulonimbus and stratocumulus observations. Measurements of power-spectrum features revealed that the first five wave numbers accounted for 79% of the total variance in cumuliform observations and 89% of the total variance in cumulonimbus observations.

Difference in overall performance between the maximum-likelihood classifier and the Bayes classifier did not vary by more than 3% no matter whether dependent or independent data was being considered or whether single-channel IR, single-channel visual, or dual-channel data was being considered or whether a 5-group or 6-group cloud-type model was considered. For dual-channel Bayes classification for the 6-group model the overall hit percentage was 76% for the dependent (design) data and 63% for the independent data; for single-channel IR Bayes classification for the 6-group model the overall hit percentage was 60% for dependent data and 57% for independent data; for single-channel visual Bayes classification for the 6-group model the overall hit percentage was 54% for dependent data and 43% for independent data. In general, classification results were better using the Bayes classifier on groups with high a priori probabilities whereas the overall hit percentage for groups with low a priori probabilities was better for the maximum-likelihood classifier than for the Bayes classifier. The major misclassifications occurred in distinguishing cumulonimbus from cirrus with lower clouds, cirrus from cumu-

lonimbus, cirrus with lower clouds from cirrus, and cumulus from clear skies. Relatively few cumulonimbus, cirrus, and cirrus with lower clouds were misclassified as clear or into one of the low-cloud groups. The pattern of errors obtained might be expected as a result of the procedure for manual classification of cloud types by the trained meteorologists. If an observation contained cumulonimbus clouds and cirriform clouds, it was labelled as cumulonimbus regardless of cloud amount of each of the two types. Also when cumulonimbus and cumulus clouds occurred in the same observation, it was labelled as cumulonimbus, and when an observation contained a small amount of cumulus cloud, it was labelled as cumulus rather than clear skies.

The overall hit percentages for the Bayes classifier applied to features extracted from single-channel, IR data, single-channel visual data, and dual-channel data are given in Table 2.3 below.

	Six-Group Model		Five-Group Model	
Channel	Dependent Data	Independent Data	Dependent Data	Independent Data
Visual	54%	43%	55%	44%
IR	60%	57%	69%	63%
Visual/IR	76%	63%	81%	69%

Table 2.3: Overall Hit Percentages of Bayes Classifier obtained by Booth [73].

Thus it can be seen that features from the single-channel IR data led to overall better classification results than could be obtained using features only from single-channel visual data. However clear skies can best be identified using single-channel visual data. Cumulus clouds were best identified by single-channel IR data. For accurate identification of cirrus clouds dual-channel data performed best.

Recommendations made by Booth for future research in cloud classification techniques included:

(1) isolation of cloud elements in an observation by use of sea-surface temperature measurements with subsequent calculation of features only on regions of an observation which contain cloud elements rather than on the entire observation

(2) addition of a "no-decision" class in which those observations whose a posteriori probability was not greater than a given threshold could be placed

(3) additional training samples for the groups of stratocumulus and cirrus with lower clouds

(4) investigation of non-parametric methods of discriminant analysis.

3.2. Cloud Segmentation

Scene segmentation refers either to the partial or complete decomposition of image data into specific parts. The simplest example of segmentation of meteorological satellite data is the separation of cloud from no cloud points. Partitioning image data into cloud-type regions is another example of segmentation. Partial segmentation of an image may result in the extraction of cloud objects or patterns such as thunderstorm cells, low-level cumulus cloud line feeder bands, or arc-shaped mesohigh boundaries.

Basic segmentation techniques for decomposition or extraction of objects include thresholding local properties, edge detection, template matching, raster tracking, and region growing. Segmentation of meteorological satellite data, either for cloud-type or cloud-pattern extraction or for observation of thunderstorm structure, has, for the most part, been the result of application of thresholding or edge detection techniques. Matching techniques have been used to track the movement of cloud patterns. Raster tracking and its variations (such as omnidirectional tracking, etc.) are employed in algorithms for line and/or curve detection. Region growing techniques start with initial partitions of an image into homogeneous regions (for example, regions of constant gray level) and then merge or split regions on the basis of some criterion for the "goodness" of a partition. Merging of partitions may continue until the gray level variance exceeds a specific threshold or may be based on more complicated semantic criteria (see Yakimowsky and Feldman [1973]).

The selection of appropriate cloud pattern thresholds is one of the most important areas of investigation for extraction of severe storm features. Parameters defining the vertical growth rate of a cell, speed-of-cell movement, presence of merging cells, and presence of splitting cells depend criti-

cally on appropriate temperature contouring of limited-scan infrared data. According to Adler [1976], "the area expansion inside particular isotherms is a more accurate and more sensitive parameter [of thunderstorm growth] in all but the very early stages" than the minimum blackbody temperature. Adler demonstrated that small areas of colder temperatures within the anvil often exhibited fluctuations associated with convective activity that were not observed in the expansion of the cirrus anvil.

Automatic selection of gray-level thresholds is usually approached by assuming that objects or patterns in an image can be characterized by modes of normal distributions in gray-level histograms. For the mode method, the threshold is selected at the bottom of a valley between two peaks. If the valley is broad and the peaks are of unequal size, a Laplacian operator can be applied to the picture to determine the gray-level value of points that lie on or near object borders. Automatic threshold selection of cloud pictures (visible data) using a Marguardt regression procedure was investigated by Yen [1974]. The procedure assumed that the gray-level distribution of the picture was a sum of normals. The success of the method was strongly dependent on the number of normal density functions (two or three) postulated. Object/background thresholds were selected at the intersections of the first and second normal density functions.

Edge detection operators have also been applied to meteorological satellite data to extract clouds from background. Smoothing or averaging the image prior to application of edge detection operators can sometimes improve the results. The Roberts digital gradient operator, which is defined for any 2 x 2 array of gray level values $\begin{matrix} A & B \\ C & D \end{matrix}$ as max ($|A-D|, |B-C|$), often performs as well as more expensive or sophisticated edge techniques on specific cloud images. Edges can also be detected by high-pass spatial frequency filtering.

The output of edge detection operators can be used in conjunction with border tracking algorithms to outline an object or the output can be used to determine a gray-level threshold (isotherm) for contouring an object.

Segmentation of infrared data into cloud-type objects by analysis of the value of the average border edge strength of connected components at each possible temperature value is discussed in Parikh [1977b]. Three edge operators were developed. Edge operators which differentiated between step edges and ramp edges were more sensitive to isolation of uniform-textured cloud patterns than operators which searched only for maximum difference between neighbors. Results of automatic threshold selection based on this hybridization of threshold and edge-detection techniques could probably be improved by procedures such as using a weighted average border-edge strength feature with less weight at border points with fuzzy edges.

Techniques for automatic selection of temperature contours for analysis of thunderstorm structure need to be developed. These techniques could be used to produce enhanced infrared imagery and to extract features which relate to severe thunderstorm activity. The selection of appropriate temperature contours could be based on analysis of features other than border-edge strength. Features such as standard deviation of temperature (within the contoured areas), uniformity of texture, mean-visible brightness, etc., should also be examined.

Streaks, curves, and lines can be detected by examining local neighborhoods (points or adjacent nonoverlapping averages of points) for line-like or streak-like patterns. Results of streak detection operations can often be significantly improved by repeating the operation more than once. A description of linear and nonlinear operators for streak and line detection can be found in Rosenfeld and Kak [1976]. Similar operators can be designed to de-

tect intersections or crossings of cloud patterns. A comparative study of curve detection operators, line detection operators, and operators for detection of branching or crossings of curves needs to be conducted in order to determine the most effective pattern recognition techniques for identification of mesohigh boundary interactions and low-level cumulus cloud-line feeder bands.

3.3. Cloud Geometry

Measures for describing geometrical properties or relationships of cloud cells form an integral part of pattern recognition algorithms for detection of severe storm features such as merging and for splitting cells, comma-shaped patterns, oval-shaped leading edges of mesohighs, and vertical growth rate of cells. Distance measures, measures of elongation, curvature measures and area measures must be specified.

The concept of merging and/or splitting cells implies that a distance measure between two cells exist. The distance between two cells can be a function, for example, of the distance between the centroids of the cells, the minimum distance between edge points, or the distance between the minimum temperatures of the cells. If merging of two cells is defined in terms of a zero distance between one or more edge points of the cells, then the recognition of merging and/or splitting cells would be dependent on the selection of an appropriate isotherm to contour the cells.

Techniques for location of comma-shaped patterns (such as thinning, thick curve following, etc.) could be developed or, alternatively, measures could be defined to detect comma-like shapes. A possible definition of a comma pattern might involve location of the medial axis of the pattern and examination of ratios of the widths to the length of the pattern.

Oval-shaped boundaries of mesohighs could be defined in terms of arcs with expected curvature values greater than a given threshold. The curvature of a point on an arc is given by the difference between the left and right slopes at the point. For an arc consisting of points $p_0, p_1, \ldots, p_n$, the left and right k-slopes at the point p_i are the directions from p_i to p_{i-k} and from p_i to p_{i+k}, respectively.

The area of a digital object is defined as the number of points in the object. In order to calculate the vertical growth rate of cells in terms of a cloud expansion parameter, appropriate isotherms for cell definition must be selected throughout the time period of observation. The selection of the warmest temperature that is unambiguously part of the entity is discussed in Adler [1976].

3.4. Cloud Tracking

The extrapolation of time-dependent features is a fundamental requirement for prediction of severe weather. Algorithms for automatic selection and tracking of cloud objects have been developed primarily for wind velocity estimation. These algorithms are reviewed in Sections 3.4.1 and 3.4.2. Automated algorithms for tracking thunderstorm cells and other similar time-varying features remain to be developed. The time-varying nature of these features distinguishes the problem of recognition of severe storm features from most current problems in pattern recognition and image processing.

3.4.1. Automatic Selection Techniques for Cloud Targets

Automatic methods for wind velocity estimation which do not rely upon the skill of a trained meteorologist to select cloud targets to be tracked from frame to frame tend to implement a particular aspect of the manual cloud-target selection procedure. Prior to manual selection of a particular individual element or feature to be traced, a meteorologist will usually assess the synoptic situation and mentally note the general cloud pattern flow over a large area. Automatic cross-correlation methods integrate cloud-pattern motion over an area (usually 32x32 or 64x64 picture points). The binary matching technique developed by Bristor [72] emulated the manual procedure of tracking cloud edges from frame to frame. As a result of factors such as evaporation, not all edges are conserved from frame to frame. In practice many meteorologists would choose to follow brightness centers (not geometric centers) of cloud masses from frame to frame rather than follow edges. The clustering algorithm of Endlich et al. [71] in which cloud data were represented by brightness centers is an analog to this procedure. Lo et al. [74] emphasized Fourier transform filtering techniques for selecting individual cloud elements of the same approximate size (preferably about 10 km) as those normally used in manual selection techniques.

The operational model of the National Environmental Satellite Service (NESS) described by Bradford et al. [72], computes cloud-displacement vectors from 64x64 cross-correlation matrices resulting from backward cross-correlation of 32x32

cloud-target areas from the second frame with 64x64 areas from the first frame. Each 32x32 array (and each 64x64 array) is centered at a five-degree latitude-longitude intersection. The choice of specific sizes for the two arrays was based on the expected speed of the clouds. The use of a smaller array for the target area than for the search area was found to improve the accuracy of cross-correlation wind velocity estimates for those areas in which clouds were moving in or out of the boundaries or in which the boundary between two different cloud patterns came inside the 64x64 grid.

Bristor [72] developed a binary matching technique for determining cloud-displacement vectors as early as 1967. A cloud edge was defined by assigning to it a brightness isopleth. The brightness range of the edge lay between the brighter values within a cloud and the darker values of the background area. The isopleth may represent actual cloud edges or it may represent a boundary where the cloud field becomes broken into elements which cannot be resolved by the satellite sensor system. Each brightness image was reduced to a binary image with cloud edges depicted by 1's and darker or brighter areas by 0's. Illustrations of typical binary images can be found in Leese et al. [71]. The procedure for computing cloud displacements from these binary images will be presented in the next section.

Endlich et al. [71] reduced cloud patterns in successive ATS-I visual images to centers of brightness whose displacement from frame to frame agreed qualitatively with cloud

motion vectors calculated manually from time-lapse data of the same scene. An ISODATA (Iterative Self-Organizing Data Analysis) algorithm was used to select the centers of brightness. ISODATA is a clustering procedure for obtaining maximum likelihood estimates for mean values (centers) with splitting and merging options for splitting clusters with too much within-cluster variability and merging clusters with too little between-cluster variability.

The program functions as follows. Scaling of the three variables -- x position, y position, and brightness value B -- is adjusted in accordance with weighting factors appropriate for the three-dimensional distance $\{\Delta x^2 + \Delta y^2 + \Delta B^2\}^{\frac{1}{2}}$ between input points. Scales chosen for x and y values ranged from 1 to 120 in increments of 4 since the original 120x120 array of satellite image points was defocused or averaged to produce a 30x30 array. The scales chosen for the brightness value ranged from 0 to 150 in steps of 10 with all points with brightness values less than 60 discarded as background elements. Then the mean value $(\bar{x}, \bar{y}, \bar{B})$ and the root mean square distance

$$r = K[\sigma^2(x) + \sigma^2(y) + \sigma^2(B)]^{\frac{1}{2}}$$

where

$\sigma^2(x)$, $\sigma^2(y)$, $\sigma^2(B)$ = variances of x, y, B, respectively,

K = sphere factor, chosen as 0.7 for this study to yield 10-15 centers per grid area

were computed from the values of all input points. The first

brightness center was specified as the mean value ($\bar{x}$, $\bar{y}$, $\bar{B}$). Data points were then compared in a sequential fashion to each brightness center in order to determine if the distance from the data point to the brightness center is less than the radius r (defined above). If the distance is less than or equal to the radius r, the data point is assigned to that cluster. Otherwise, if the distance from every brightness center is greater than the radius r, the point is chosen as a new center. After all points have been processed, a new set of brightness centers (mean values of clusters) is computed for each group.

At this stage, splitting and lumping options can be applied. For splitting, the standard deviations within each group for each of the variables x, y, B are computed and the group having the largest value for any one dimension is tentatively split through its mean value. New centers are computed, and if the distance between the two new centers is greater than some parameter θ_C, the two new clusters replace the original one. For lumping, if two cluster centers are closer than θ_C, the two clusters are merged into one. It was found experimentally that the splitting and merging operations did not improve the accuracy of cloud motion vectors. The next stage in the ISODATA program was to discard all centers that had less than θ_N members, where θ_N was set equal to three for this application. The MOTION program matched brightness centers on two pictures and computed distances between matched pairs.

Lo et al. [74] applied low-pass filters, band-pass filters,

and high-pass filters of various sizes to Fourier transforms of successive satellite pictures in order to separate cloud components of different sizes and discard cloud elements which are too large to move passively with the wind. In a limited region clouds of different sizes tend to occur at different altitudes and consequently represent different motion vectors. Results from studies on simulated and real-cloud data revealed that the filtering technique did not significantly improve wind velocity vectors for multi-layered, mixed-motion cloud regions. The filtering technique failed to categorize cloud size by wavelength. High-frequency components contained information not only about small clouds but also about sharp edges of large clouds and similarly low-frequency components contained information not only about large cloud masses but also about small clouds with low contrast and/or blurred edges. Different filters or different approaches to the problem were suggested for future research. In particular, thresholding processes to separate different cloud types, enhancement procedures such as two-tone cloud/background images to yield sharper cross-correlation peaks, and multispectral cloud-classification methods were expected to improve wind velocity estimates for multi-layered fields.

3.4.2. Automatic Techniques for Tracking Cloud Targets

Automatic techniques for wind-velocity estimation such as cross correlation, Euclidean norm, and phase difference calculate a cloud displacement vector from the brightness measurements of a given sector. For these techniques, the entire sector is chosen as the cloud target to be tracked from frame to frame. Cross-correlation methods can be modified by selection of a subset of the given sector to be correlated with a sector from the second image of the same size as the given sector. Phase difference and cross-correlation Fourier methods can be modified by filtering a Fourier transform prior to calculation of a cloud-displacement vector. Binary matching techniques and iterative fitting techniques compute a cloud displacement vector from cloud features or cloud targets derived from the brightness measurements of the given sector, i.e., from edge features and brightness centers, respectively.

For cross-correlation techniques a cloud displacement vector, represented by a displacement index of p picture elements in the x-direction (direction of ascending columns) and a displacement index of q picture elements in the y direction (direction of ascending rows), is defined by the pair of indices (p', q') for which the correlation coefficient $R(p', q') = \max[R(p,q)]$ for all p, q where $-P \leq p \leq P$ and $-Q \leq q \leq Q$. The values of P and Q are determined from consideration of reasonable values for cloud displacements. If $\bar{F}$ and $\bar{G}$ are the means respectively of a sector f(i,j), for $i=1,\ldots,n_i$ and $j=1,\ldots,n_j$ from the first image and a sector

$g(i,j)$, for $i=1,\ldots,n_i$ and $j=1,\ldots,n_j$ from the second image, then the correlation coefficient $R(p,q)$ is defined as

$$R(p,q) = \frac{Cov(p,q)}{\sigma_f \sigma_g}$$

where

$$Cov(p,q) = \frac{1}{\{(n_i-p)(n_j-q)\}-1} \sum_{j=1}^{n_j-q} \sum_{i=1}^{n_i-p} [f(i+p,j+q)-\bar{F}][g(i,j)-\bar{G}]$$

$$\sigma_f = \{ \frac{1}{n_i * n_j - 1} \sum_{j=1}^{n_j} \sum_{i=1}^{n_i} [f(i,j)-\bar{F}]^2 \}^{\frac{1}{2}}$$

$$\sigma_g = \{ \frac{1}{n_i * n_j - 1} \sum_{j=1}^{n_j} \sum_{i=1}^{n_i} [g(i,j)-\bar{G}]^2 \}^{\frac{1}{2}}$$

Speed-of-cloud motion and angle-of-cloud motion is trivially calculated as shown in the next section from the displacement values (p',q').

Computation of a cross-correlation matrix of 25x25 lag values (p,q) required approximately ten minutes on the IBM System 360 Model 50, according to Leese et al. [71]. The computation time can be greatly reduced by using fast Fourier transform methods to compute the cross-covariance $Cov(p,q)$. Since the Fourier transform of the cross-covariance of two functions is the product of the complex conjugate of the Fourier transform of one of the functions with the Fourier transform of the other function, the inverse Fourier transform of this product will then yield the cross-covariance function. Time

required to compute a 64x64 cross-correlation matrix on the IBM 360/50 by the fast Fourier transform methods, search for the maximum value, and print out the results was only thirty seconds as compared to ten minutes for the direct method.

Fast Fourier transforms compute sums of products of two image matrices at different lag positions. These sums can be used to calculate the dot product between two vectors (cross correlation) or the distance between two vectors (Euclidean norm). Advantages of the Euclidean norm technique mentioned by Phillips and Smith [72] are its high degree of flexibility and readily interpretable results.

The GOES simulation model for wind velocity estimation at the National Environmental Satellite Service uses a first-guess displacement in combination with direct computation of cross-correlation coefficients to obtain a cloud-displacement vector. The computer program, which is specifically adapted to operate as efficiently as fast Fourier transform methods on the CDC-6600, calculates an initial set of about 100 values of cross-correlation coefficients in the neighborhood of the first-guess location rather than the entire set of 4096 coefficients for a 64x64 matrix. If the displacement determined from the initial set of 100 values matches the first-guess field for the cloud-motion vector (which is derived from cloud-height information coupled with wind field profiles from the National Meteorological Center), the cloud displacement is accepted. The initial matching threshold was 45 degrees in direction and 5 meters per second in speed. If the displace-

ment vector does not match the first-guess field, the entire matrix of cross-correlation coefficients is computed.

Although cross-correlation could be applied to the binary-edge pictures constructed by Bristor's [72] binary matching technique described in the previous section, processing time requirements were about equal or slightly less for cloud displacement calculation from match scores of the sector from the first image with every possible (or reasonable) sector from the second image. The origin of the cloud-displacement vector was defined as the center of the first sector. The number of positions containing 1's in both the sector from the first image and a sector from the second image formed the match score. The terminus of the cloud-displacement vector was defined as the center of the sector from the second image with highest match score. The method was critically dependent upon the equivalence of the brightness slice in the two sectors. If it were possible to calibrate and normalize the data for solar illumination, methods such as the binary matching technique or ISODATA technique which depend upon thresholds to determine cloud edges or cloud masses could be used operationally to compute cloud-displacement vectors, according to Leese [64].

A program called MOTION, developed at Stanford Research Institute and described by Endlich et al. [71], matched ISODATA brightness centers in two successive frames by iterating on a fitting function F. F measured the distance $\{(\Delta x-\overline{\Delta x_k})^2 + (\Delta y-\overline{\Delta y_k})^2 + (\Delta B)^2\}^{\frac{1}{2}}$ between the displacement

vector for any two centers taken from successive frames and an input displacement vector ($\overline{\Delta x_k}$, $\overline{\Delta y_k}$, 0) with x displacement $\overline{\Delta x_k}$, y displacement $\overline{\Delta y_k}$, and brightness displacement of zero. The initial values $\overline{\Delta x_k}$ and $\overline{\Delta y_k}$ were specified as the median displacement in the x direction and the median displacement in the y direction respectively taken over all pairs of centers with the first center in picture 1 and the second center in picture 2. The pair of centers for which F was smallest was then considered to be a matched pair. The matching procedure continued for centers not previously matched by searching again for the smallest value of F. The matching procedure terminated either when there were no more centers to be matched or when the value of F exceeded a predetermined threshold value chosen in this case to be representative of a departure from the input displacement vector of approximately $10\,m \cdot sec^{-1}$. For the next iteration and for every succeeding iteration of F values, the input displacement values $\overline{\Delta x_k}$ and $\overline{\Delta y_k}$ were chosen as average values of x displacements and y displacements for matched pairs only. In the cases investigated by Endlich et al. [71], only three iterations were necessary for stable results in pair matching.

Approaches for selecting ISODATA brightness centers other than applying ISODATA techniques to the two successive pictures independently were analyzed. It was found that movement of groups of clouds across boundaries in some cases presented problems when using the independent analysis approach for successive frames. It was then decided to use the centers on

the first picture as an initial guess for centers on the second picture; this worked well if the general displacement was not too large in comparison with the average distance between brightness centers. The approach finally adopted used an initial estimate of the general displacement to reposition the brightness centers from picture 1 as initial guess centers for picture 2. The initial estimate of the general displacement was obtained as follows. Splitting commands of ISODATA applied independently to the two pictures transformed 1 center into 2, then 4, then 8 centers for each picture. The MOTION program matched as many as possible of the 8 centers from picture 1 with centers from picture 2. The average x and y displacements of these matched pairs determined the initial estimate of the general displacement.

The ISODATA brightness centers, which represent cloud data within an area having a certain radius, yielded averaged motion vectors appropriate for use in synoptic-scale numerical forecasting. Difficulties were encountered in applying the ISODATA technique to large, dense, cloud bands such as the intertropical convergence zone in which a variety of cloud motions with few distinct discernible features could be seen. The human eye tends in these cases to follow any individual, small, recognizable features which are conserved from frame to frame rather than average the pattern into 10-15 brightness fields. To improve the accuracy of cloud-displacement vectors for multi-layered cloud regions, the addition of infrared measurements to form a four-dimensional input vector for the

ISODATA program was suggested.

Lo and Parikh [73] compared a Fourier cross-correlation method and a Fourier phase difference method for estimation of cloud-displacement vectors on a variety of simulated cloud data. Simulated conditions included change of brightness, change of size, cloud rotation, edge effects (cloud elements moved out of the edge of one picture but similar clouds did not come in at the opposite edge of the second picture), mixed motion, and random instrumental noise.

The phase difference method is based on the assumption that the second picture $g(x,y)$ represents a linear shift of p units in the x direction and q units in the y direction from the first picture $f(x,y)$, i.e.,

$$g(x,y) \equiv f(x-p,y-q) \text{ for all } x,y$$

The Fourier transform $H(u,v)$ of the cross-covariance function $h(x,y)$ of two pictures $f(x,y)$ and $g(x,y)$ is given by

$$H(u,v) = G(u,v)^* \cdot F(u,v)$$

where

$G(u,v)^*$ = complex conjugate of Fourier transform of the second picture $g(x,y)$

$F(u,v)$ = Fourier transform of the first picture $f(x,y)$

From the definition of the Fourier transform and the assumption that $g(x,y) = f(x-p,y-q)$, it can be seen that

$$G(u,v) \equiv \int_{-\infty}^{\infty}\int_{-\infty}^{\infty} g(x,y)\, e^{-2\pi i(ux+vy)}\,dxdy$$

$$= \int_{-\infty}^{\infty}\int_{-\omega}^{\omega} f(x-p,y-q)\, e^{-2\pi i(ux+vy)}\,dxdy$$

$$= \int_{-\infty}^{\infty}\int_{-\infty}^{\infty} f(x',y')e^{-2\pi i[(x'+p)u+(y'+q)v]}\,dx'dy'$$

$$= F(u,v)e^{-2\pi i(pu+qv)}$$

If $F(u,v)$ is expressed in terms of its amplitude and phase angle as

$$F(u,v) = ||F(u,v)||e^{-i\varphi_f(u,v)}$$

then

$$G^*(u,v) = ||F(u,v)||e^{i[2\pi(pu+qv)-\varphi_f(u,v)]}$$

and

$$H(u,v) = G^*(u,v)\cdot F(u,v) = ||F(u,v)||^2 e^{2\pi i(pu+qv)}$$

The phase angle $\varphi_h(u,v)$ for $H(u,v)$ is given by

$$\varphi_h(u,v) = 2\pi(pu+qv)$$

The shifts p and q can be determined from successive u and v values respectively from the relations

$$\varphi_h(u+1,v) - \varphi_h(u,v) = 2\pi p$$

$$\varphi_h(u,v+1) - \varphi_h(u,v) = 2\pi q$$

When the phase difference method and the cross-correlation method were applied to simulated, mixed-motion data which violated the basic assumption of linear shift (i.e., $g(x,y) \neq f(x-p,y-q)$ for any p,q), neither the phase difference method nor the cross-correlation method could be analyzed to obtain true estimates for both types of motion. Filtering in the frequency domain or thresholding in the spatial domain were suggested as possible approaches for future research.

3.4.3. Automatic Computation of Wind Velocity

The output from automatic techniques for tracking cloud targets is a displacement vector (p',q'). Speed $|\bar{c}|$ and direction 0 of cloud motion are calculated as follows:

$$|\bar{c}| = \frac{[(p' \cdot \Delta x)^2 + (q' \cdot \Delta y)^2]^{\frac{1}{2}}}{\Delta t}$$

$$0 = \arctan \frac{p' \cdot \Delta x}{q' \cdot \Delta y}$$

where

Δx, Δy = sampling intervals of the input picture matrix in the east-west and north-south directions, respectively

Δt = time interval between the two pictures

The automated models of the National Environmental Satellite Service (NESS) for estimation of low-level cloud motion vectors have incorporated an automatic post-editor as a major part of the quality control unit. The post-editor of the ACLOWIN-XL1 model of NESS rejects a low-level cloud motion vector as invalid if it satisfies either of the following climatological criteria:

(1) its magnitude is greater than 40 kts,

(2) it has a westerly component and is located between 20°N and 20°S.

The post-editor of the GOES simulation model of NESS considers criteria such as displacement from the first-guess field, horizontal consistency between neighboring cloud-motion vectors,

and gradient around the primary maxima of the cross-correlation field for determination of the validity of low-level cloud-motion vectors.

AD-A042 446 L N K CORP SILVER SPRING MD F/G 4/2
SEVERE STORM PATTERN RECOGNITION FROM METEOROLOGICAL SATELLITE --ETC(U)
JUN 77 L N KANAL, J A PARIKH DAAG29-76-D-0100

UNCLASSIFIED ECOM-77-3 NL

2 OF 2
AD
A042 446

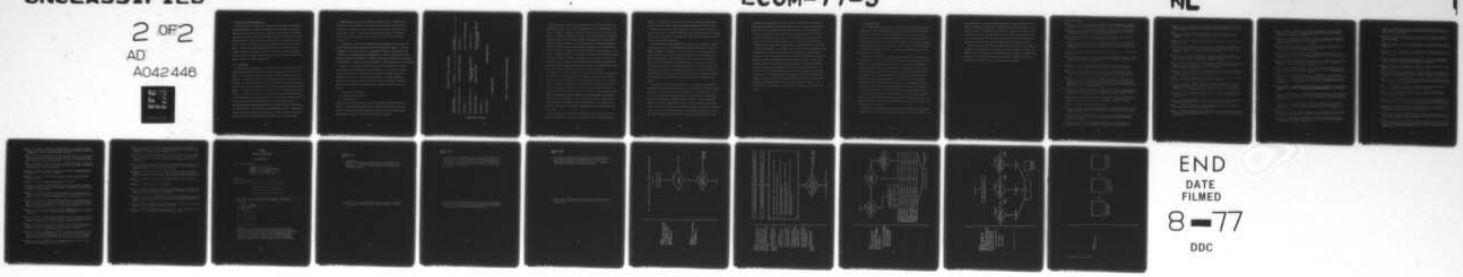

END
DATE FILMED
8-77
DDC

4. Conclusions and Recommendations

The purpose of this study was to assess the current status of pattern recognition techniques for severe storm features and to consider the potential applicability of pattern recognition techniques to the automatic identification and prediction of severe weather phenomena from satellite data. In the previous sections of this report, we have reported in some detail on the nature of severe storm features obtainable from visible and infrared satellite data. We have also described the past developments and current status of automatic techniques related to cloud classification and weather phenomena. In this section, we summarize our conclusions and recommend directions which appear fruitful for further investigation.

4.1. Conclusions

In the last decade automatic pattern recognition and image processing techniques for analysis of meteorological satellite data have been directed primarily toward solution of cloud classification and wind-velocity estimation problems. The resolution and spectral characteristics of the meteorological satellite data controlled the type of information which could be automatically extracted from the data and the nature of applicable pattern-recognition techniques. For coarse resolution data, point-by-point classification schemes were developed. With the availability of high-resolution scanning radiometer data, decision-tree models based on extraction of cloud-type features were constructed. Critical thresholds for either point-by-point classification schemes or decision-tree models were determined either from design samples, from theoretical considerations, or from conventional meteorological sources. Cloud-shape and texture features could be determined from visible data only. Successful cloud-type classification schemes required multispectral satellite data.

Geosynchronous satellite data formed the primary input to automatic wind-velocity estimation programs. Cross-correlation techniques were applied to two successive windows of either infrared or visible data to determine cloud-displacement vectors. Techniques to extract wind estimates from displacements confined to individual thermal slices are currently under investigation at NESS.

The automatic cloud-classification models and automatic wind-velocity estimation models have been extensively tested only over oceanic regions. The non-homogeneity of the land surface as a background coupled with an increase in the influence of local meteorological phenomenon which result in non-advective cloud motions, complicates the problem of automatic-cloud type and wind-velocity analysis over land areas. The success of these systems on a global scale has yet to be tested.

Automatic severe weather identification and forecasting models place even more stringent requirements than automatic-cloud type or wind-velocity models on the amount and nature of meteorological satellite data which must be considered by the system. In assessing the potential of pattern-recognition techniques to identify severe storm features from satellite data, we observed that severe-storm features could generally be grouped into three major categories:

1) wind-dependent features
2) enhanced-infrared features
3) visual features.

Specific severe weather features in each of the above categories are listed in Table 2. Wind-dependent features and enhanced-infrared features (with the possible exception of steepest temperature gradient and top heights) require time sequences of data to track the evolution of the feature.

CATEGORIES OF SEVERE STORM FEATURES

SEVERE STORM FEATURES

ENHANCED INFRARED	VISIBLE	WIND DEPENDENT
STEEPEST TEMPERATURE GRADIENT	MESOHIGH BOUNDARY INTERACTIONS	UPPER-LEVEL JET
TOP HEIGHTS		RIGHT OR LEFT DEVIATING STORMS
VERTICAL GROWTH RATE OF CELL	LOW-LEVEL CUMULUS CLOUD-LINE FEEDER BANDS	LOW-LEVEL VORTICITY
SPEED-OF-CELL MOVEMENT	BRIGHT AND TEXTURED	UPPER-LEVEL DIVERGENCE AND LOW-LEVEL CONVERGENCE
MERGING CELLS		
SPLITTING CELLS		PENDANT-SHAPED CELLS
OVERSHOOTING TOPS		

Table 2. Categories of Severe-Storm Features.

Relationships of specific severe-storm features to either wind data, enhanced infrared data, or visible data suggested by Table 1 represent one and only one approach to recognition and quantitative measurement of severe-storm features. Alternative relationships exist. Automatic techniques to identify pendant-shaped cells, for example, could be formulated based on cell-shape measurements rather than on veer of wind with height. Although overshooting tops were categorized under enhanced infrared features, the resolution of infrared SMS data is too coarse to delineate individual overshooting tops. Outlines of individual tops are best observed in higher resolution visible imagery for a low-sun angle. The major disadvantage of using visible data to track overshooting tops is that a relatively expensive normalization procedure for solar zenith angle would be necessary before statistical relationships between top brightness and severe-weather phenomena could be developed.

Our general conclusion in examining the current status of severe-storm identification is that it is an area of individual, subjective experience which exists in the form of verbal descriptions of various features. As a result, there are differences of opinion among meteorologists concerning the nature of the data necessary for identification of particular severe weather features and the role of automatic processing in forecasting severe weather phenomena. Although most of the responses to our severe weather questionnaire indicated a need for automatic processing of high resolution, time sequences of visible and infrared meteorological satellite data in an interactive environment, the blend of man-machine interaction envisioned within these systems varied.

On the one hand, it is said that automatic procedures cannot hope to compete with computerized methods when dealing with local phenomena over small

regions. A meteorologist can quickly assess the relevance of ground-based reports, teletype reports, radar, and satellite features and bring to bear his expertise on the limited area of concern. In this view, the role for automated techniques is in dealing with more global situations where vast amount of data are to be handled in order to define the small percentage of areas on which a human should concentrate.

On the other hand, image processing of large amounts of satellite data on a sequential computer is not economically feasible at the present time. The general procedure to handle large amounts of data is to partition the data into smaller regions (windows) and base decisions on local operations performed on each window. This procedure fails to give satisfactory results when contextual information from nearby windows is necessary for a decision or when given features lie in two different windows. As a consequence, many meteorologists prefer to use automatic techniques to exhaustively examine small regions which they have selected in order to detect and measure subtle differences and changes which are not easily measured by the human visual system.

It would seem that a more careful study of the interaction between human and machine processing of weather data will be facilitated by whatever attempts are made in automating some of the severe storm features in Table 2. As a first step, descriptions of severe weather features should be standardized so as to allow automatic extraction whenever feasible. For wind-dependent features in Table 2, algorithms to extract low-level and upper-level wind vectors over oceanic areas and to determine divergence and vorticity (Thomasell [1977]) are being investigated at NESS. Our extensive search of the literature and our questioning of individuals working on different aspects of me-

teorological data processing revealed no existing algorithms for automatic extraction of enhanced infrared and visible imagery of severe storm features. While many pattern recognition algorithms and image processing algorithms exist for the various low-level operations that would be involved in extraction of these features (see Section 3), a comparative study of the applicability of relevant algorithms does not exist. To determine the best algorithms relative to these features would require experimentation with real data.

As mentioned earlier, in the pattern recognition and image processing literature almost no attention has been paid to the extraction of features which evolve with time. This time variation of enhanced infrared severe storm features has not been attacked previously using pattern recognition techniques, and any demonstration of feasibility on these features would lend credence to pattern recognition approaches for severe-storm pattern recognition. If these features could be automatically observed and extracted, this would substantially aid in rapid decision making concerning severe storm activity and testing correlations between measurements from satellite-derived severe-storm features and from ground-based reports on severe weather phenomena. For this reason, it is worthwhile to consider the development of automatic techniques.

4.2. Recommendations

It is recommended that an attempt be made to quantify current verbal descriptions of severe-storm features in order to minimize ambiguity of definition and to facilitate (a) comparative studies of the correlation of the various features to severe-weather phenomena and (b) the automatic extraction of those features which correlate well with specific severe-weather phenomena. Implementation of this recommendation will require close and extended interaction with meteorologists active in severe-storm identification and prediction from satellite data.

The key to the automation of many of the potentially useful severe-storm features lies in being able to detect and recognize patterns which evolve in time. It is important to establish as early as possible the feasibility of automatically recognizing such patterns. It appears that it may be possible to recognize some of these patterns using limited scan infrared data. In the event that it should prove feasible to automatically extract time-varying patterns as recommended above, it would be desirable to conduct a comparative study of curve-detection operators and line-detection operators for identification of mesohigh-boundary interactions and low-level cumulus cloud-line feeder bands. In line with the above, it is recommended that initially work be done on merging or splitting cells in infrared data enhanced in a manner similar to that currently being used for human recognition. For this investigation, data which contains well-defined events of the type to be recognized will be needed.

Algorithms for wind-velocity estimation and calculation of divergence and vorticity fields over ocean areas are being developed at NESS. There are cur-

rently differences of opinion among meteorologists on the feasibility of using automatic techniques to calculate cloud displacements which represent the ambient wind flow. The applicability of automatic algorithms to determine wind-veclocity vectors from cloud displacements over land has not been determined. In the event that they are applicable, these programs could be incorporated into automatic methods to extract wind-dependent severe-storm features.

Decision trees (similar to that of Scofield's) which make use of a number of features to determine specific severe-storm activity should be developed. In developing these trees, particular attention should be given to features whose extraction is likely to be successfully automated. Interactive programs for the design of such decision trees should also be considered.

List of References

Adler, R. F. (1976), "Thunderstorm monitoring from a geosynchronous satellite", Preprint volume, 7th Conference on Aerospace and Aeronautical Meteorology.

Anderson, R. K., et al. (1974), "Application of meteorological satellite data in analysis and forecasting", ESSA Technical Report NESC 51, including supplement, November 1971, and supplement #2, March 1973.

Arking, A. (1964), "Latitudinal distribution of cloud cover from TIROS III photographs", Science, Vol. 143, No. 3606, pp. 569-572.

Auvine, B., and D. N. Sikdar (1973), "Satellite derived upper level dynamical features near the jet stream on two severe storm days", Space Science and Engineering Center, University of Wisconsin, Annual Report 1973, NG-26-72, pp. 150-155.

Battan, L. J. (1961), Nature of Violent Storms, Doubleday and Co., Garden City, New York.

Blum, H. (1962), "An associative machine for dealing with the visual field and some of its biological implications", Air Force Cambridge Research Laboratories, Bedford, Mass., AFCRL-62-62.

Booth, A. L. (1972), "Cloud classification of mapped satellite imagery by discriminant analysis and perceptron methods", Unpublished manuscript.

Booth, A. L. (1973), "Objective cloud type classification using visual and infrared satellite data", Institute for Fluid Dynamics and Applied Mathematics, University of Maryland, College Park, MD, Technical Note BN768.

Bradford, R., J. Leese, and C. Novak (1972), "An experimental model for the automated detection, measurement, and quality control of low-level cloud motion vectors from geosynchronous satellite data", Proc. of the 8th International Symposium on Remote Sensing of Environments, University of Michigan, Ann Arbor, Michigan, October 2-6, 1972.

Bristor, C. L. (1972), "Extracting atmospheric wind estimates from geostationary satellite image data", Proc. of Symposium on Computer Image Processing and Recognition, Columbia, Missouri, August 1972, Paper No. 2-1.

Burgess, D. W., and R. A. Brown (1973), "The structure of a severe right-moving thunderstorm: New single doppler radar evidence", preprint volume, 8th Conf. on Severe Local Storms, Denver, Colorado, October 15-17, 1973.

Charba, J. B. (1976), Personal communication.

Clark, R. M. (1976), "The East Coast winter storm, 1-2 February, 1976, a case study", National Weather Service/National Environmental Satellite Service, S.A.I. Note 76/8.

Computer Sciences Corporation (1976), "Storms at ground system concept study", Contract NAS 5-11999, Task Assignment 707; Goddard Space Flight Center, Greenbelt, Maryland.

Conover, J. H. (1962), "Cloud interpretation from satellite altitudes", Air Force Cambridge Research Laboratories, Bedford, Mass., AFCRL-62-680.

Darling, E. M., Jr., and R. D. Joseph (1968), "Pattern recognition from satellite altitudes", IEEE Trans. on Systems, Science and Cybernetics, Vol. SSC-4, No. 1, pp. 38-47.

Doswell, C. A., and J. T. Schaeffer (1976), "On the relationship of cirrus clouds to the jet stream", Monthly Weather Review, Vol. 104, No. 1, pp. 105-106.

Edinger, J. G. (1967), Watching for the Wind, Doubleday and Co., Inc., Garden City, New York.

Endlich, R. M., D. E. Wolf, D. J. Hall, and A. E. Brain (1971), "Use of a pattern recognition technique for determining cloud motions from sequences of satellite photographs", Journal of Applied Meteorology, Vol. 10, No. 1, pp. 105-117.

Greaves, J. R., and D. T. Chang (1970), "Technique development to permit optimum use of satellite radiation data", Goddard Space Flight Center, Greenbelt, MD, Final Report on NASA Contract N62306-69-C-0227.

Gruber, A. (1975), "Comments on 'Correlation between cloud thickness and brightness using Nimbus 4 THIR data (11.5 μm channel) and ATS 3 digital data'", Journal of Applied Meteorology, Vol. 14, pp. 643-644.

Gurka, J. J. (1976), "Satellite and surface observations of strong wind zones accompanying thunderstorms", preprint volume, 6th Conf. on Weather Forecasting and Analysis, Albany, New York, May 10-14, 1976.

Holroyd, E. W. (1971), "Lake-effect cloud bands as seen from weather satellites", Journal of Atmospheric Sciences, Vol. 28, pp. 1165-1170.

Hunter, H. E., and N. H. Kemp (1971), "Final report for application of Avco data analysis and prediction techniques (ADAPT) to prediction of cyclone present motion and 12-hour motion, and re-centering effects, using Nimbus HRIR data", Avco Corporation, Systems Division, Contract AVSD-0334-71-RR.

Kanal, L. N. (1972), "Interactive Pattern Analysis and Classification Systems: A Survey and Commentary", Proc. IEEE, Vol. 60, No. 10, October 1972, pp. 1200-1215.

Kanal, L. N. (1974), "Patterns in Pattern Recognition: 1968-1974", IEEE Trans. on Information Theory, Vol. IT-20, No. 6, November 1974, pp.697-722.

Kanal, L. N. (1975), "Prospects for Pattern Recognition; Report on a Survey and Workshop", NSF-EIA-U. of Md. Report, 1975.

Kanal, L. N. (1977), "On hierarchical classifier theory and interactive design", to appear in Applications of Statistics, P. R. Krishnaih (ed.), North-Holland Publishing Co.

Katz, Y. H. (1964), "Pattern recognition of meteorological satellite cloud photography", Proc. of the Third Symp. on Remote Sensing of Environment, University of Michigan, Ann Arbor, Mich.

Koffler, R., A. G. DeCotiis and P. K. Rao (1973), "A procedure for estimating cloud amount and height from satellite infrared radiation data", Monthly Weather Review, Vol. 101, No. 3, pp. 240-243.

Kulkarni, A. V. (1976), "Optimal and heuristic synthesis of hierarchical classifiers", Ph.D. dissertation, University of Maryland, Computer Science Technical Report Series, TR-469, August 1976.

Kulkarni, A. V., and L. N. Kanal (1976), "An optimization approach to hierarchical classifier design", Proc. 3rd International Joint Conf. on Pattern Recognition, San Diego, Calif., November 1976.

Leese, J. A. (1964), "Quantitative interpretation of low-level cumuliform cloud patterns as seen in meteorological satellite videographs", ESSA Contract CWG-10795, University of Michigan, Ann Arbor, Mich.

Leese, J. A., C. S. Novak and V. R. Taylor (1970), "The determination of cloud pattern motions from geosynchronous satellite image data", Pattern Recognition, Pergamon Press, Vol. 2, pp. 279-292.

Leese, J. A., W. Pickel, B. Goddard, and R. Brower (1971), "An experimental model for automated detection, measurement and quality control of sea-surface temperatures from ITDS-IR data", Proc. of the 7th International Symp. on Remote Sensing of Environment, Univ. of Michigan, Ann Arbor, Mich., May 17-21, 1971.

Liou, K. (1975), "Can the changes in cloud thickness be monitored from satellite-brightness measurements?", Journal of Applied Meteorology, Vol. 14, pp. 644-645.

Lo, R. C., J. Mohr, and J. A. Parikh (1974), "Applications of fourier transform methods of cloud movement estimation to simulated and satellite photographs", Computer Science Technical Report Series, University of Maryland, College Park, TR-292.

Lo, R. C., and J. A. Parikh (1973), "A study of the application of fourier transforms to cloud movement estimation from satellite photographs", Computer Science Technical Report Series TR-247, University of Maryland, College Park, Md.

Mancuso, R. L., and R. M. Endlich (1973), User's Manual Wind Editing and Analysis Programs--Spherical Grid, Stanford Research Institute, 20 pp.

Mathews, M. D., and E. C. Johnston (1976), "Midwest severe weather outbreak of December 13-14, 1975", National Weather Service/National Environmental Satellite Service, S.A.I. Note 1/76-2.

Miller, J. A. (1976), "An example of dry line convective development 'The Omaha Tornado'", National Weather Service/National Environmental Satellite Service, S.A.I. Note 76/12.

Miller, D. B. (1971), "Automated production of global cloud-climatology based on satellite data", U.S. Air Force Air Weather Service Technical Report 242, pp. 291-306.

Miller, D. B., and R. G. Feddes (1971), Global Atlas of Relative Cloud Cover, 1967-70, Washington, D.C., U. S. Department of Commerce and U. S. Air Force, pp. 1-8.

Miller, D. B., J. A. Leese, and C. L. Bristor (1975), "Further outlook for GOES", U. S. Dept. of Commerce, Washington, D.C., NOAA Technical Memo. NESS-64, March 1975.

Miller, R. C. (1972), "Notes on analysis and severe-storm forecasting procedures of the Air Force Global Weather Central", Tech Report 200 (Revised Feb. 25, 1975), Air Weather Service (MAC), USAF, May 1972.

Mosher, F. R. (1976), "Cloud height determination", Proc. of the 19th Plenary Meeting of COSPAR, Philadelphia, Pa., June 8-19, 1976.

Oliver, V. J., and J. F. W. Purdom (1974), "Mesoscale convective processes in the tropics as revealed by satellite imagery", Preprint volume, 5th Conf. on Weather Forecasting and Analysis, St. Louis, Missouri, March 4-7, 1974.

Oliver, V. J., and R. A. Scofield (1976), "Estimation of rainfall from satellite imagery", preprint volume, 6th Conf. on Weather Forecasting and Analysis, Albany, New York, May 10-14, 1976.

Parikh, J. A. (1977a), "A comparative study of cloud classification techniques", Remote Sensing of Environment (to be published).

Parikh, J. A. (1977b), "Automatic cloud classification and segmentation", Ph.D. dissertation, Computer Science Center, University of Maryland, College Park (in press).

Park, S. U., D. N. Sikdar, and V. E. Suomi (1974), "Correlation between cloud thickness and brightness using Nimbus 4 THIR data (11.5-μm channel) and ATS 3 digital data", Journal of Applied Meteorology, Vol. 13, pp. 402-410.

Parmenter, F. C. (1976), "A near-stationary Gulf of Alaska low--its effect on weather in the Pacific northwest", National Weather Service/National Environmental Satellite Service, S.A.I. Note 3/76-2.

Parmenter, F. C., and R. K. Anderson (1974), "Mesoscale details in synoptic scale systems", preprint volume, 5th Conf. on Weather Forecasting and Analysis, St. Louis, Missouri, March 4-7, 1974.

Phillips, D. R., and E. A. Smith (1972), "Digital matching techniques applied to cloud displacement measurement and pattern tracking", Proc. of Symp. on Computer Image Processing and Recognition, Columbia, Missouri, August 1972. Paper No. 2-2.

Purdom, J.F.W. (1974), "Satellite imagery applied to the mesoscale surface analysis and forecast", preprint volume, 5th Conf. on Weather Forecasting and Analysis, St. Louis, Missouri, March 4-7, 1974.

Purdorm J.F.W. (1976a), "Some uses of high resolution GOES imagery in the mesoscale forecasting of convection and its behavior", preprint volume, 6th Conf. on Weather Forecasting and Analysis, Albany, N.Y., May 10-14, 1976.

Purdom, J.F.W. (1976b), "The use of GOES 1 km resolution imagery in helping pinpoint tornado activity", National Weather Service/National Environmental Satellite Service, S.A.I. Note 76/15.

Rosenfeld, A. (1965), "Automatic cloud interpretation", Photogrammetric Engineering, Vol. 31, No. 6, pp. 991-999.

Rosenfeld, A., and A. C. Kak (1976), Digital Picture Processing, Academic Press, New York.

Savage, R. C. (1977), Personal communication, 9 Feb. 1977.

Scofield, R. A. (1975), "Infrared imagery used for tracking the 26 November snowstorm", National Weather Service/National Environmental Satellite Service, S.A.I. Note 12/75-3.

Scofield, R. A. (1976), "Satellite pictures used for locating the rainfall associated with a convective system over Texas", National Weather Service/National Environmental Satellite Service, S.A.I. Note 76/18.

Scofield, R. A., and C. E. Weiss (1976), "Application of synchronous meteorological satellite (SMS) products and other data for short-range forecasting in the Chesapeake Bay region", preprint volume, 6th Conf. on Weather Forecasting and Analysis, Albany, N.Y., May 10-14, 1976.

Shenk, W. E., and R. J. Curran (1973), "A multi-spectral method for estimating cirrus cloud top heights", Journal of Applied Meteorology, Vol. 12, pp. 1213-1216.

Shenk, W. E., and R. J. Holub (1972), "A multispectral cloud type identification method using Nimbus 3 MRIR measurements", Proc. of the Conf. on Atmospheric Radiation, Fort Collins, Colorado, August 7-9, 1972.

Shenk, W. E., R. J. Holub, and R. Neff (1976), "A multispectral cloud type identification method developed for tropical ocean areas with Nimbus 3 MRIR measurements", Monthly Weather Review, V104, pp. 284-291.

Shenk, W. E., and V. V. Salomonson (1971), "A simulation study exploring the effects of sensor spatial resolution on estimates of cloud cover from satellites", U.S. National Aeronautics and Space Administration, Goddard Space Flight Center, Greenbelt, MD, NASA Technical Note NASA TN D-6247.

Simpson, J., and W. L. Woodley (1971), "Seeding cumulus in Florida: New 1970 results", Science, Vol. 172, pp. 117-126.

Smith, W. L., and P. K. Rao (1972), "Sea surface temperature measurements from satellites", Proc. of the 5th Symp. on Temperature, Its Measurement and Control, Washington, D. C., June 21-24, 1972.

Smith, W. L., P. K. Rao, R. Koffler and W. R. Curtis (1970), "The determination of sea-surface temperature from satellite high resolution infrared window radiation measurements", Monthly Weather Review, Vol. 98, No. 8, pp. 604-611.

Stamm, A. J., and T. H. Vonder Haar (1970), "A study of cloud distribution using reflected radiance measurements from the ATS satellite", Journal of Applied Meteorology, Vol. 9, No. 3, pp. 498-507.

Stockman, G. C., and Kulkarni, A. V. (1976), "Maryland Interactive Pattern Analysis and Classification System: User Documentation", University of Maryland, Computer Science Technical Report Series, TR-482, September 1976.

Sutton, O. G. (1961), The Challenge of the Atmosphere, Harper & Brothers, New York.

Thomasell, A. (1977), Personal communication.

Wang, P. P., and R. T. George, Jr. (1974), "Bibliography on tornado research", Tech. Report TR-74-01, NASA Research Grant NSG-5020, Dept. of Electrical Engineering, Duke University, August 1974.

Yakimovsky, Y., and J. A. Feldman (1973), "A semantics-based decision theory region analyzer", Proc. of 3rd International Joint Conf. on Artificial Intelligence, pp. 580-588.

Yen, H. H. (1974), "Threshold selection techniques 3", University of Maryland, Computer Science Technical Report Series, TR-294.

Young, M. T. (1975), "The GOES wind operation", U. S. Dept. of Commerce, Washington, D. C., NOAA Technical Memo. NESS-64, March 1975.

APPENDIX

Severe Storm Questionnaire

QUESTIONNAIRE

Please send responses to:

Professor Laveen Kanal
Laboratory for Pattern Analysis
Department of Computer Science
University of Maryland
College Park, Maryland 20742.

YOUR NAME: _____

ADDRESS & TEL. NO. _____

_____

_____

_____

1. What are the categories of severe weather? (Some examples are listed below. What additional categories should be listed?)

   1. Severe windstorm
   2. Heavy rainstorm
   3. Hailstorm
   4. Tornado
   5. _____
   6. _____
   7. _____
   8. _____
   9. _____

2. Corresponding to the above categories, please list the important characteristics (features) of each of these categories which you think may be obtainable from SMS satellite data; e.g., splitting cells, pendant shaped cells, overshooting thunderstorm tops, right moving storms, low-level cumulus feeder bands, mesohigh boundary interactions, steepest temperature gradient, speed of cell motion, vertical rate of cell growth,

2. (Continued)
pattern of upper level and lower level convergence and divergence. If possible, please list the features for each category in the order of their importance for characterizing each category.

3. Which of the above characteristics do you feel are amenable to computer extraction from visible and IR satellite data?

4. For each of the characteristics listed under question 3, we would like to know your opinion as to whether or not that characteristic can be extracted from a single IR image. If not, are visible imagery and/or a sequence of visible and/or IR images required? If so, how many images and at what intervals do you suggest?

5. Do you know of algorithms which exist or are under development for computer extraction of such features? If so, please provide references to the algorithms and to the laboratories or persons who can be contacted concerning them.

6. Are there algorithms which you feel should be implemented either for preprocessing meteorological satellite data or for analyzing specific severe storm areas? Do you feel that such areas will have to be pin pointed by a meteorologist using a man-machine interactive system?

7. Do you have specific suggestions on how computers can best help in severe storm weather pattern recognition using satellite data?

STEP 1.
Examine shape of cloud to determine if convective (round, oval, carrot-shaped, triangular).
USE VIS AND IR.

STEP 2.
Determine if convection is deep.
USE ENHANCED IR.

FIG. 1. Decision Tree for Convective Rainfall- R.Scofield, NESS, 1977

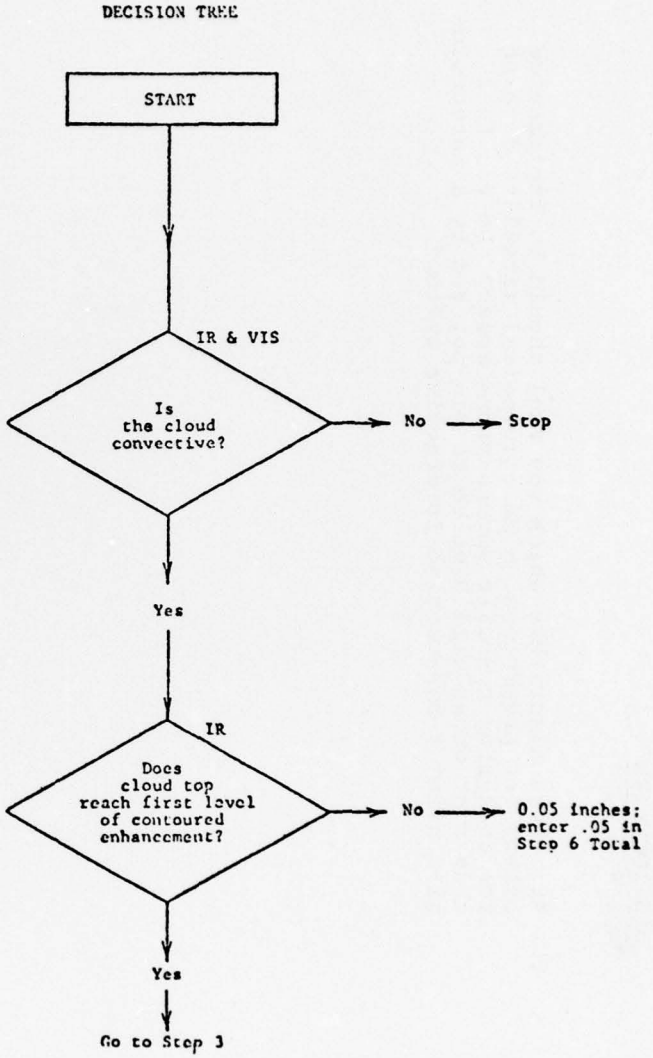

STEP 3.
Identify the active portion of the convective cloud system. Use enhanced IR and VIS. VIS (underlined) means that visible imagery is the best data for making that decision.

A. Upwind portion of anvil locates the active area of the convective system:

IR gradient is tightest around upwind end of anvil.

Clouds are brightest and sometimes textured at upwind end.

Comparison of two successive pictures shows motion of anvil edge; greatest in downwind direction.

Winds aloft (usually best at 300 mb) used for determining upwind direction.

B. Overshooting tops show active area of anvil.

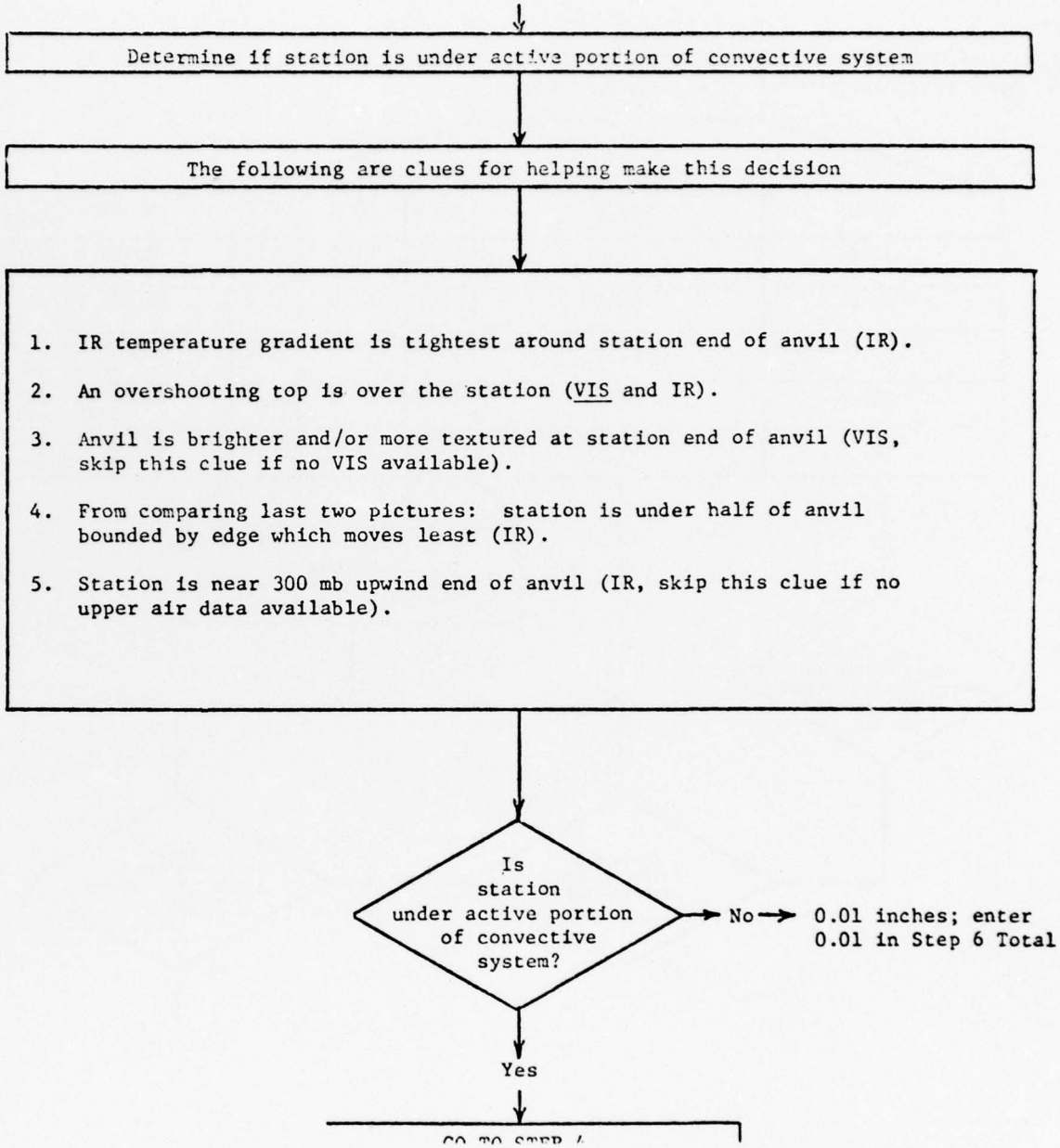

TEP 4.
stimate half-hourly recip rates as a unction of cloud top emperature and tempera-ure change.
SE ENHANCED IR.

- Rainfall is heaviest when and where clouds are still getting colder and coldest area is growing.

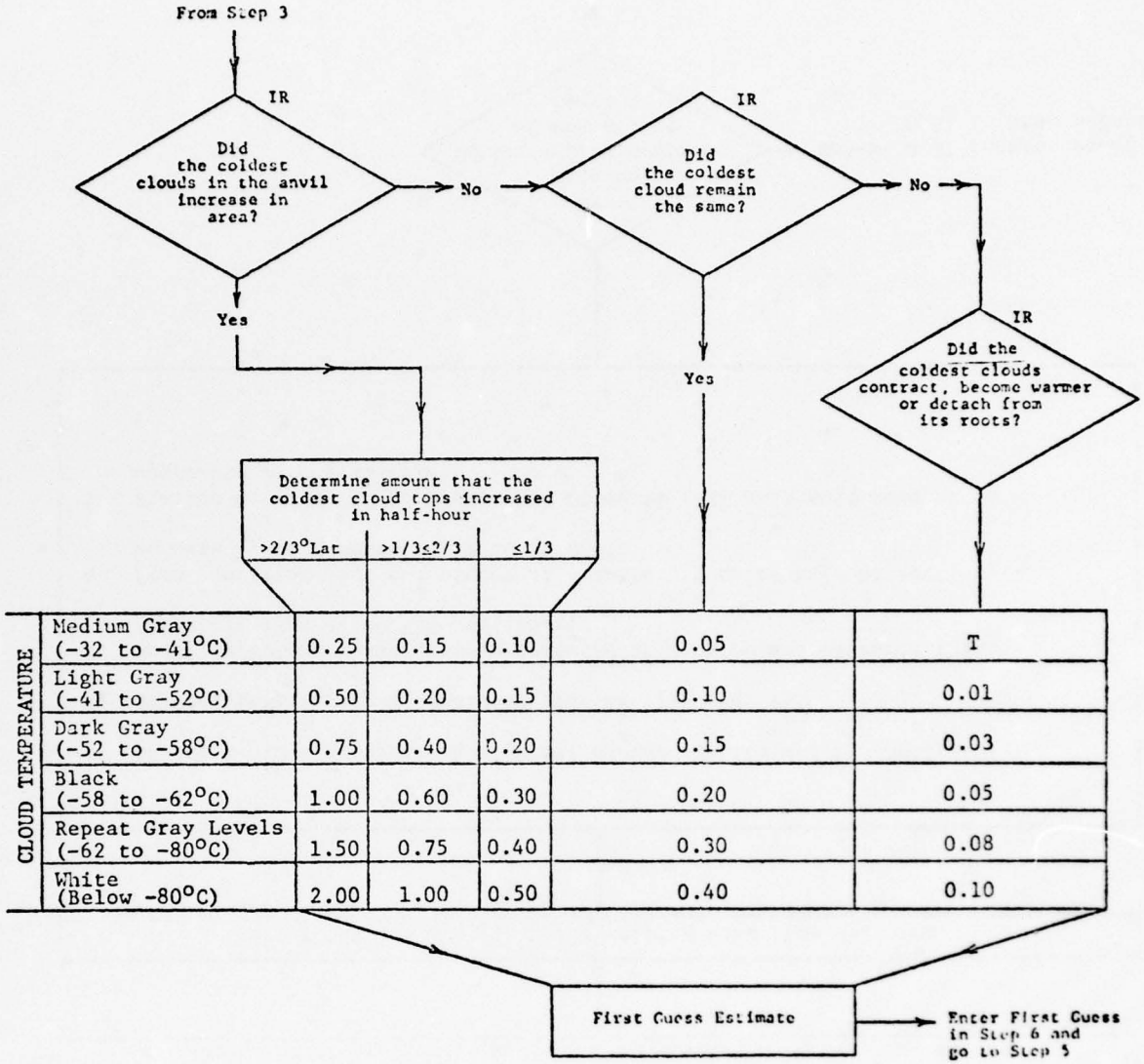

STEP 5.
Analyze imagery for presence of precip amplifiers.
USE VIS AND ENHANCED IR.
VIS (underlined) means that visible imagery is the best data for making that decision.

Overshooting tops.

Cell mergers.

Line mergers.

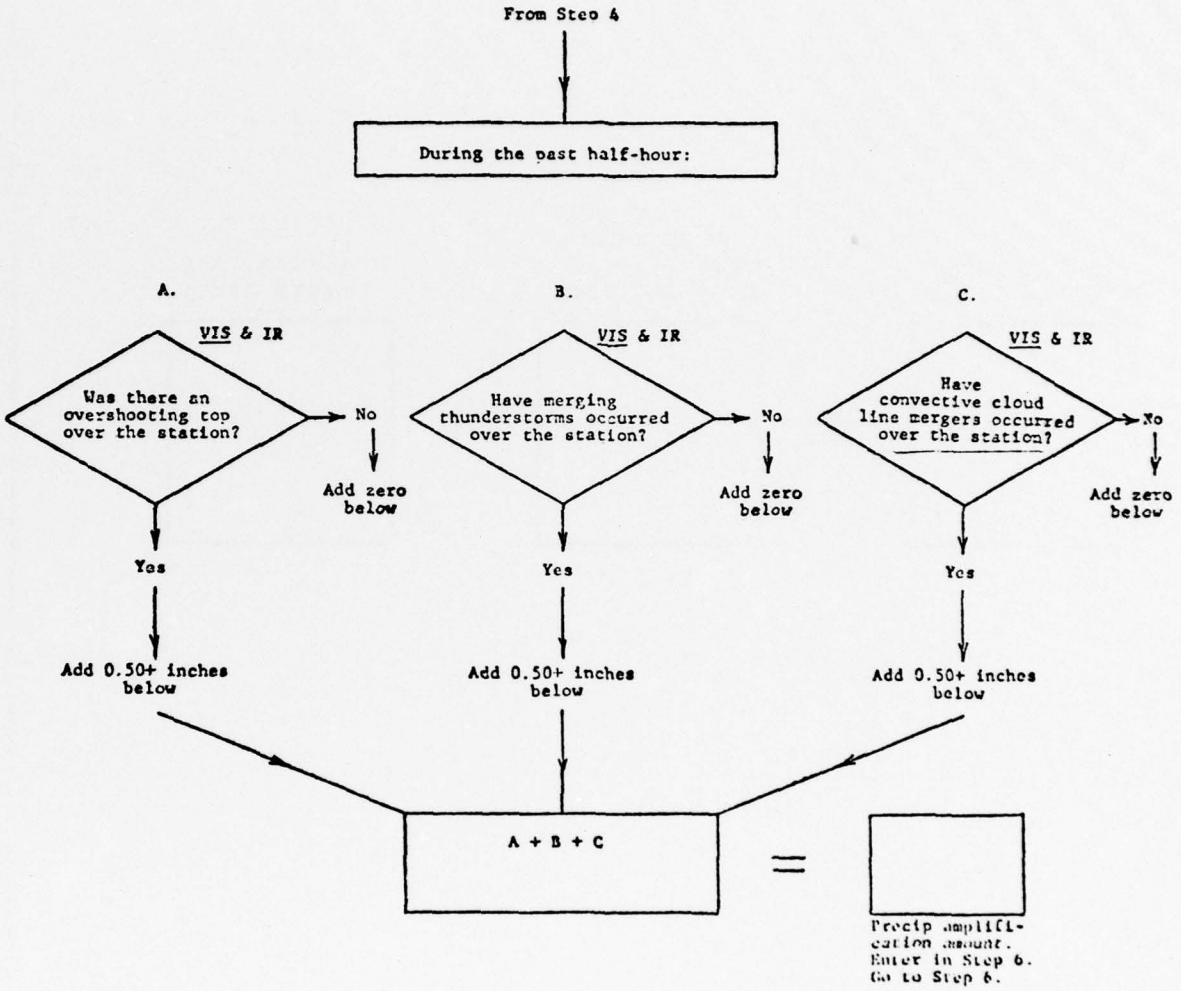

☆U.S. GOVERNMENT PRINTING OFFICE: 1977 777-022/2

STEP 6.
Total Estimate.

First guess from Step 4.

Precipitation amplification amount from Step 5.

Total Estimate (Steps 2, 3)